UPPSALA
UNIVERSITET

Simulating ion transport in electrolyte materials with physics-based and machine-learning models

YUNQI SHAO

Dissertation presented at Uppsala University to be publicly examined in Polhemsalen, Ångströmlaboratoriet, Lägerhyddsvägen 1, Uppsala, Wednesday, 14 December 2022 at 09:15 for the degree of Doctor of Philosophy. The examination will be conducted in English. Faculty examiner: Professor Barbara Kirchner (University of Bonn).

Abstract
Shao, Y. 2022. Simulating ion transport in electrolyte materials with physics-based and machine-learning models. *Digital Comprehensive Summaries of Uppsala Dissertations from the Faculty of Science and Technology* 2210. 55 pp. Uppsala: Acta Universitatis Upsaliensis. ISBN 978-91-513-1642-0.

Electrolytes are indispensable components of electrochemical devices such as batteries, fuel cells, and supercapacitors, and the mass transport in electrolytes is one of the most important design focuses of such devices. A microscopic picture of ion transport is essential to link the chemical properties of electrolyte materials to their electrochemical applications. This thesis aims to establish such a connection through computer simulations of the transport phenomena, using a combination of physics-based and machine-learning methods.

The first part of the thesis concerns the study of transport phenomena with molecular dynamics simulations, where the atomistic interactions are described by physics-based classical force fields. Guided by the principles of non-equilibrium statistical mechanics, the simulations reveal governing factors of ion transport in different systems. This is exemplified by the leading contribution of hydrodynamic interactions in the non-ideal ionic conductivity, and the qualitative distinction between transient and long-lived ion pairs. This approach also aids the interpretation and comparison of experiments and simulations, by elucidating their intrinsic constraints imposed by the reference frame, and their proper inter-conversions.

The second part of the thesis aims to remedy a major limitation of the physics-based approach, namely the difficulty of accurately simulating complex reactive systems. The machine learning methods were developed to systematically generate the models from electronic structure calculations. The strength of this approach is demonstrated by showing how it correctly predicted the transport coefficients of proton-conducting materials with the desired accuracy. Limitations of this data-driven approach are also investigated, demonstrating the potential pitfall in the parameterization process, and leading to the development of an adaptive learn-on-the-fly workflow.

Overall, the present thesis showcases how computer simulations can lead to insights regarding the ion transport in electrolyte materials, and how the development of machine-learning methods could empower those simulations to tackle complex and reactive systems.

Keywords: electrolytes, ionic conductivity, ion transport, molecular dynamics, machine learning potential, proton transfer

Yunqi Shao, Department of Chemistry - Ångström, Structural Chemistry, Box 538, Uppsala University, SE-751 21 Uppsala, Sweden.

List of papers

This thesis is based on the following papers, which are referred to in the text by their Roman numerals.

I   Y. Shao, K. Shigenobu, M. Watanabe, and C. Zhang, "Role of viscosity in deviations from the Nernst–Einstein relation", J. Phys. Chem. B **124**, 4774–4780 (2020);

II   H. Gudla, Y. Shao, S. Phunnarungsi, D. Brandell, and C. Zhang, "Importance of the ion-pair lifetime in polymer electrolytes", J. Phys. Chem. Lett. **12**, 8460–8464 (2021);

III   Y. Shao, H. Gudla, D. Brandell, and C. Zhang, "Transference number in polymer electrolytes: mind the reference-frame gap", J. Am. Chem. Soc. **144**, 7583–7587 (2022);

IV   Y. Shao, M. Hellström, A. Yllö, J. Mindemark, K. Hermansson, J. Behler, and C. Zhang, "Temperature effects on the ionic conductivity in concentrated alkaline electrolyte solutions", Phys. Chem. Chem. Phys. **22**, 10426–10430 (2020);

V   Y. Shao, M. Hellström, P. D. Mitev, L. Knijff, and C. Zhang, "PiNN: a Python library for building atomic neural networks of molecules and materials", J. Chem. Inf. Model. **60**, 1184–1193 (2020);

VI   Y. Shao, F. M. Dietrich, C. Nettelblad, and C. Zhang, "Training algorithm matters for the performance of neural network potential: a case study of Adam and the Kalman filter optimizers", J. Chem. Phys. **155**, 204108 (2021);

VII   Y. Shao and C. Zhang, "Adaptive on-the-fly parameterization of neural network potentials for liquid electrolyte: application to protic ionic liquids", Manuscript in preparation (2022).

Reprints were made with permission from the publishers.

The author's contribution to the papers

In all the listed papers, I participated in the scientific discussion, experiment design and manuscript preparation. I also carried out most of the computer code implementation, the simulation, and the data analysis, specifically:

Paper I   molecular dynamics simulation and the analysis;
Paper II   the analysis code, and analysis for the NaCl/aq system;
Paper III   the analysis code, and the theoretical derivation;
Paper IV   molecular dynamics simulation and the analysis;
Paper V   the atomic neural network code, and benchmarks for the QM9 and the water dataset;
Paper VI   the algorithm code, and most of the numerical simulation;
Paper VII   the workflow code, and most of the numerical simulation.

List of publications not included in the thesis

- Y. Shao, L. Knijff, F. M. Dietrich, K. Hermansson, and C. Zhang, "Modelling bulk electrolytes and electrolyte interfaces with atomistic machine learning", Batter. Supercaps. **4**, 585–595 (2021);
- Y. Shao, L. Andersson, L. Knijff, and C. Zhang, "Finite-field coupling via learning the charge response kernel", Electron. Struct. **4**, 014012 (2022).

Contents

Glossary

1. Introduction

1.1 Phenomena in electrochemical cells

Advances in materials and energy sources shape the modern society. In a much-electrified society, its sustainability depends on its control over electricity, materials, and their interplay. Solutions to many of the pressing problems, e.g., energy sources, energy storage, and efficient energy conversion, are found in electrochemical cells (batteries, fuel cells, and electrolysis cells, to name a few).[1,2]
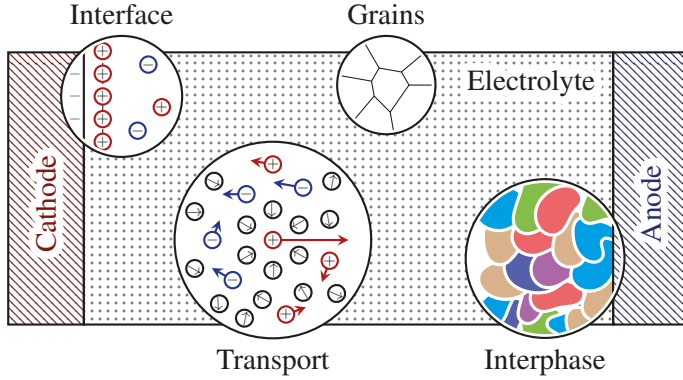
Figure 1.1. An electrochemical cell (in open circuit) and some of the many phenomena in it.

The operation of an electrochemical cell is the interplay of a number of factors, from the interfacial structure[3] and its impact on electrochemical reactions[4] to the formation of solid electrolyte interphases;[5] from the transport of mass, heat, and momentum to the mechanical deformation and degradation of the cell, as illustrated in Fig. 1.1. Each of those factors is coupled intricately with one another, and an understanding or rational design of those devices would require integrated knowledge on different levels.

1.2 Multiscale modelling of electrochemical cells

The multiscale models emerge as the phenomena are characterized and described at different domains.[6] For example, an electrochemical cell may be characterized by its current response to a frequency-dependent voltage via

electrochemical impedance spectroscopy (EIS). The EIS can be interpreted in terms of different parts of the cell in the form of its equivalent circuit model.[7] Each component may be further modelled as continuums of materials and interfaces in between.[8] The interfacial and bulk properties find their origin in atomistic or electronic structures, to be characterized by atomistic simulations or spectroscopic, diffraction, and microscopic measurements.

Such a hierarchical structure benefits the research in several ways. Going up the hierarchy, the implication of low-level phenomena at a higher level can be envisioned or simulated, providing the mechanisms for interpretation or prediction. Walking down the hierarchy, the empirical observations may be traced back to their origins as a means to judge the fundamental laws or the approximations made along the path. Overall, the multiple scales represent the existence of apt physical laws or equations for certain aspects of the phenomena, while the missing links between them call for empirical or theoretical advances.[6]

With the recent development of data-driven models and the much increased throughput of experimental and computational data, it is not hard to imagine that such methods could alleviate the difficulties in the above physics-based hierarchy, of "bridging" different scales. Example usage of the so-called machine learning (ML) models include the automated inference of empirical rules,[9] or as surrogate models in lieu of their more expensive counterparts for large-scale screening[10] or atomistic simulations.[11]

In the context of multiscale modelling, this thesis chose the specific problem of ion transport in electrolytes. That said, it is the hope of the author that this work contributes to a clear connection between the bulk properties of the electrolyte and the atomistic interactions for better predictions, better understandings, and better designs of the electrochemical cell.

1.3 Ion transport in electrolytes

Given their role as ion conductors in cell operation, the ion transport properties of electrolytes are among the most important factors to consider in cell design. In the search for novel electrolyte materials, under the constraints of, e.g., electrochemical (thermal) stability and mechanical properties, a wide range of materials attract interest.[12–14] The quest for understanding and improving their transport properties challenges the experiments, the theory, as well as the simulations of electrolytes.

Accurate measurements of transport coefficients, i.e., ionic conductance, transference number, and diffusion coefficient, have been available for liquid electrolytes since the early 1900s.[15] Methods and theories based on potentialstatic polarization extend the availability to systems as solid polymer electrolytes.[16] The advance in experimental techniques, notably nuclear magnetic resonance (NMR) measurements, enable the direct mobility measure-

ments for individual ions (self diffusion) with pulse-field gradient (PFG)-NMR,[17] or certain ionic species with electrophoretic NMR.[17] Observations made in those experiments are not always easy to understand, and the correct interpretation and elucidation of the data require theoretical support.

Classical theories of liquid electrolytes, such as Ostwald's law[18] or the Debye-Hückel-Onsager theory,[19,20] succeeded in relating transport properties to other thermodynamic quantities for dilute electrolytes. Despite remarkable theoretical developments such as the mean spherical approximation,[21,22] the hypernetted chain approximation,[23] or the classical density functional theory,[24,25] the mathematical intricacy and the necessary simplification limit their applications to idealized systems, and employing them in realistic problems remains challenging.[9,26–28]

In more general cases, a first estimation of the transport properties may be given by its viscosity, giving rise to the Walden rule in the study of ionic liquids.[12] An adjusted Walden relation, where the radius of ion is taken into account, formed the base of many discussions regarding ion transport.[29] There, an "ideal" conductivity is derived from the self-diffusion coefficients with the Nernst-Einstein relation. Given the complete set of transport coefficients, the deviation of ionic conductivity from the ideal relation may be attributed to correlations between ions.[30–33] Although derivation through the aforementioned theoretical framework is still difficult, computer simulations offer the possibility to verify hypotheses.

Simulations at the atomistic/electronic level provide much of the information unavailable in the previous discussion. In molecular dynamics (MD) simulations, factors such as ion pairing and association[34–38] can be gauged, and their effects in terms of the ion correlations[39–41] can be directly evaluated. MD simulations also provide detailed structural information[42] and thermodynamic properties[43] of the model system which could be used to enhance the theoretical models with inversion procedures.[44]

Introduction of electronic structure to MD simulations further enables the investigation of transport phenomena involving chemical reactions like proton transfer (PT),[45–48] ion-ion charge transfer,[49] etc. To reach the full potential of this combination, ML models can be built to bypass the electronic structure calculation and accelerate the MD, so that the desired quantities can be converged,[50–53] which is also developed in this thesis.

1.4 Scope of this thesis

This thesis focuses on the simulation of electrolyte materials at an atomistic scale and the specific problem of their ion transport properties. Within the hierarchical structure of multiscale modelling, the aim is clear — to bridge the phenomena of transport with the dynamics of atoms. Specifically, the following questions will be answered in this thesis: (1) How does the ion

transport relate to the microscopic motion of atoms? (2) What are the insights into the ion transport that emerge from the microscopic view? (3) How do interatomic forces affect the atomistic dynamics and the ion transport?

Using classical force fields, the first part of the thesis deals with the first two questions. Those were studied before computer simulations became feasible, and simulation mainly serves to check the validity of those theories, that is, to show their applicability for given systems and to clarify their connection to experimental measurements. Sec. 2.1 gives a brief review of the development of ion transport theories, and Sec. 2.2 introduces principles of MD simulations. Chapter 3 contains three studies focusing on different systems and concepts in ion transport.

Sec. 3.1 showcases the computation of transport coefficients with two typical electrolytes NaCl/aq and [BMIM][PF$_6$], where an inspection of the finite size effect in MD simulations reveals the role of hydrodynamic interaction in ion transport (Paper I). Sec. 3.2 turns to the concept of ion pairing and shows the importance of lifetime in the interpretation of ion pairing for the polymer electrolyte PEO-LiTFSI (Paper II). Finally, Sec. 3.3 stressed reference frame (RF) as the conceptual gap to be bridged for the comparison between experimental and simulation results in the same polymer electrolyte system (Paper III).

Classical force fields fall short in regard to the final question, especially in treating chemical reactions. Chapter 4 attacks the problem with a ML approach, with the basics of using ML potentials introduced in Sec. 2.3. Sec. 4.1 showcases the strength of the combination of neural network potentials (NNPs) and MD in the study of transport properties of NaOH/aq, where Grotthuss-type PT contributes to its high ionic conductivity (Paper IV).

Further development of the methodology to cater to more complex systems is presented in Sec. 4.2 (Paper V). During the method development, a possible pitfall is noted regarding the transferability of NNPs, and the role of the training algorithm is highlighted in Sec. 4.3 (Paper VI). An adaptive learn-on-the-fly (LOTF) workflow is designed to mitigate the issue and rigorously study the coupling between sampling and training procedures, the workflow and its application to the protic ionic liquid (PIL) [C$_1$IM][HOAc] is discussed in Sec. 4.4 (Paper VII).

2. Theory and Method

2.1 Theory of ion transport in electrolytes

As outlined in the introduction, ionic transport is the central property of electrolytes, such that being "ionic conductors and electronic insulators" becomes the modern definition of electrolytes.[54] By focusing on ionic transport, the following response relation between the flux density $\mathbf{J}_\alpha$, and the gradients of molar concentration c_α and potential Φ, will be studied at its linear limit:*

$$\mathbf{J}_\alpha = \mathbf{J}_{\alpha,\text{migration}} + \mathbf{J}_{\alpha,\text{diffusion}} \tag{2.1}$$

$$= -\frac{t_\alpha}{q_\alpha N_\mathrm{A}} \sigma \nabla \Phi - D \nabla c_\alpha \tag{2.2}$$

where σ is the ionic conductivity, t_α and q_α are transference number and the formal charge of species α, D is the salt diffusion coefficient, and N_A is the Avogadro constant.

Electrolytes, termed by Faraday[56] to explain the phenomena of ionic conduction, were recognized by Arrhenius[57] as substances that dissociate into charged particles upon solution. This microscopic picture of electrolytes is pivotal to a mechanistic understanding of their structures, reactivities and transport properties of interest here.[15] The following section shows how those transport coefficients are related to the microscopic motions of ions, as a cornerstone of this thesis.

2.1.1 Phenomenology of ion transport

The identification of ion formation upon solvation, rather than electrolysis, marks the first hint that the phenomena of ion conduction can be characterized by its equilibrium state. Following Einstein's seminal work on Brownian motion,[58] the driven motion of a particle and the random motion are related through a common "mobility" u_α or self-diffusion coefficient D_α^s of the particle, characterized by its mean squared displacement (MSD):

$$u_\alpha = \frac{D_\alpha^\mathrm{s}}{RT} = \lim_{t \to \infty} \frac{1}{6RTt} \left\langle \frac{1}{N_\alpha} \sum_{i \in \alpha} \|\Delta \mathbf{r}_i(t)\|^2 \right\rangle \tag{2.3}$$

---

* Such a simplified form requires some clarification: firstly, the asserted linear relation is expected at small currents, which is the case for typical measurement of transport properties.[55] For the same reason, the isolated effect of an electrochemical driving force is studies here, albeit convection or coupling with heat flux might be of interest at the device scale.

where R is the gas constant, T is the temperature, and $\Delta\mathbf{r}_i(t)$ is the displacement of particle i over time t, with which the flux of a species becomes:

$$\mathbf{J}_\alpha = u_\alpha c_\alpha \mathbf{X}_\alpha = -u_\alpha c_\alpha \nabla \bar{\mu}_\alpha \tag{2.4}$$

where we consider migration and diffusion as the result of a common driving force $\mathbf{X}_\alpha$, as the negative gradient of the electrochemical potential $\bar{\mu}_\alpha = \mu_\alpha + q_\alpha N_A \phi$, with μ_α being the chemical potential of species α, and ϕ being the electrostatic potential (not to be confused with Φ).*

This representation asserts that $\mathbf{J}_\alpha$ only arises from $\mathbf{X}_\alpha$, which is only valid at low concentration. A more general form of the linear relation is known as the Onsager phenomenological equations:†

$$\mathbf{J}_\alpha = \sum_\beta \Omega_{\alpha\beta} \mathbf{X}_\beta \tag{2.5}$$

and the correlation function may be derived from the linear response theory,[65] in an analogous form as the MSD:

$$\Omega_{\alpha\beta} = \lim_{t\to\infty} \frac{1}{6k_B T V N_A^2 t} \left\langle \Delta\mathbf{r}_\alpha(t) \cdot \Delta\mathbf{r}_\beta(t) \right\rangle \tag{2.6}$$

where the total displacement of α particles in the system is denoted as $\Delta\mathrm{r}_\alpha$, k_B is the Boltzmann constant, V is the system volume, and $\Omega_{\alpha\beta}$ is the so-called Onsager coefficients.

The implication of such a relation between the microscopic fluctuation of the particle and macroscopic transport coefficients is worth a few remarks: above all, the law of motion for the particles sets the constraints for the macroscopic coefficients.[66] As an example, the time-reversibility of the microscopic dynamics implies the symmetry of Onsager coefficients ($\Omega_{\alpha\beta} = \Omega_{\beta\alpha}$) known as the Onsager reciprocal relation (ORR).[61] Further, the form of equations may be cast back to the form of Eq. (2.1):[59]

$$\sigma = \sum_{\alpha\beta} q_\alpha q_\beta N_A^2 \Omega_{\alpha\beta}^0 \tag{2.7}$$

$$t_\alpha^0 = \sum_\beta q_\alpha q_\beta \Omega_{\alpha\beta}^0 / \sigma \tag{2.8}$$

and in the specific case of 1:1 binary electrolytes:

$$D^0 = \frac{2RT}{c} \cdot \left(1 + \frac{d\ln y}{d\ln c}\right) \cdot \frac{\left(\Omega_{+-}^0\right)^2 - \Omega_{++}^0 \Omega_{--}^0}{\Omega_{++}^0 + \Omega_{--}^0 - 2\Omega_{+-}^0} \tag{2.9}$$

---

* For the the distinction between the potential definitions and the possible ambiguity, see eqs. (43–45) in ref. 59, or the discussion in ch. 12 of ref. 60.

† Several alternative forms exists at this level, such as the inverse Onsager equations,[59,61,62] the Maxwell-Stefan equations,[63] or the modified version by Newman.[64] Given that they all describe the same process, they can be converted from one to another, and the choice is usually a matter of convenience.

where c is the salt concentration and y is the molar activity coefficient.

This connection allows for the rigorous experimental validation of theoretical estimations, including the ORR.[67] Notably, the transport coefficients here are presented under the solvent-fixed frame of reference (denoted as 0), conversion between different RFs is again constrained, and its implication is detailed in Paper III.

2.1.2 Conceptual models of ion transport

In the previous section, the theoretical discussion is restricted to a phenomenological level — the derivation depends merely on the simple assumption of a linear relation. The simplicity leads to rigidity rather than triviality of its consequence. That said, no quantitative prediction of the transport coefficients is yet arrived, which will be provided by conceptual models in the following.

While those models are not applied in this thesis, the concepts they provided will help with the interpretation of experimental and simulation results. The theoretical development and derivation go beyond the scope of this thesis, the interested reader is directed to the comprehensive account by Justice.[68, pp. 226]

Following Arrhenius' theory of ion dissociation, ionic conductivity is naturally related to the degree of ionization, which also corresponds to the Van 't Hoff "anomalies" regarding the osmotic pressures of aqueous electrolytes.[18] The mass action law, suggested by Ostwald, entails the concentration c dependency of the molar conductivity $\Lambda = \sigma/c$ as:

$$\frac{1}{\Lambda} = \frac{1}{\Lambda_0} + \frac{1}{K_d}\frac{\Lambda}{\Lambda_0^2}c \tag{2.10}$$

where Λ_0 the limiting molar conductivity at infinite dilution, and K_d is the dissociation constant of the electrolyte. Given the abundance and accuracy of conductivity measurements, they become a useful gauge to study ion-solvent interactions in electrolytes.[15, ch. 6] However, despite the success and simplicity of Eq. (2.10), it fails to account for a number of electrolytes known as "strong electrolytes", where the Kohlrausch's measurements give a square root dependency of conductivity to the concentration:

$$\Lambda = \Lambda_0 - A\sqrt{c} \tag{2.11}$$

The observation is clarified first by the recognition that strong electrolytes are completely dissociated ($K_d \to \infty$),[68, pp. 227] and then the Debye-Hückel-Onsager (DHO) theory, which derived the square root law from the electrostatic interactions between ions. The DHO theory quantifies the effect of ion interactions on transport properties through time-averaged quantities centred on an ion of type α, namely the spatial distribution functions of β particles:

$g_{\alpha\beta}(\mathbf{r})$, the $\mathbf{r}$ dependent mean velocity of β: $\mathbf{v}_{\alpha\beta}(\mathbf{r})$, and the $\mathbf{r}$ dependent mean force between α and β particles: $\mathbf{f}_{\alpha\beta}(\mathbf{r})$.*

Those quantities are mutually coupled through interatomic interactions and continuity equations, and simplification is necessary to reach a solvable set of equations. Debye and Hückel solved $g_{\alpha\beta}(\mathbf{r})$ and its perturbation upon an electric field with a linearized Poisson-Boltzmann equation, and obtained a change of the driving force felt by the central ion ($\Delta\mathbf{X}$), known as the *relaxation effect*. Another effect that is later discussed by Onsager, is the perturbation to $\mathbf{v}_{\alpha\beta}(\mathbf{r})$ due to the driving force acting on the central ion following Stoke's Law, known as the *electrophoretic effect*.[20] The two effects can generally be combined to arrive at flux density in the form:[70]

$$\mathbf{J}_\alpha = c_\alpha \sum_\beta (u_\alpha \delta_{\alpha\beta} + \Omega'_{\alpha\beta})(\mathbf{X} + \Delta\mathbf{X}) \tag{2.12}$$

where $\delta_{\alpha\beta}$ is the Kronecker delta, Ω' accounts for the electrophoretic effect typically given by the Oseen tensor, and $\Delta\mathbf{X}$ accounts for the relaxation effect. This gives the DHO limiting law of conductivity in the form of Eq. (2.11).

Whether the Ostwald or the DHO law holds depends on the type of electrolytes, and it raises some conceptual difficulties when some strong electrolytes (like NaCl) exhibit different behaviour depending on the solvent, where the mass action law is unexpected.[68, pp. 228] Bjerrum attributed this to the oversimplification of the linearized Poisson-Boltzmann equation, who went on and suggested treating short-range ion-pair configurations as neutral species, which does not interact with the rest of ions.[71]

It's worth mentioning that Bjerrum's concept of ion pair is a bypass of the mathematical difficulty rather than a claim of the actual dynamics,[71] or as put by Onsager: "a convenient but reasonable convention" when "the recombination kinetics is too fast for a sharp definition".[18] The distinction between long-lived ion pairs and those with fast kinetics becomes significant when the full set of transport coefficients (such as the complete set of Onsager coefficients) are considered, as demonstrated in Paper II.

2.2 Molecular Dynamics Simulations

The above relations between transport coefficients and correlation functions permit their direct determination through computer simulations, which becomes possible with the rapidly increased computing power in the past few decades. This section gives a brief overview of the numerical simulation of MD, with some special focus on its connection to transport properties.

---

* See pp. 234–239 of Ref. 68 for more detailed definitions and derivations. The distinction between this point of view to that in Sec. 2.1.1 resembles that between the Lagrangian and Eulerian specification of flow fields.[69]

With the assumption that the motions of nuclei and electrons can be treated separately, i.e., the Born-Oppenheimer (BO) approximation, the problem is decoupled to the determination of potential energy U as a function of nuclei positions $\mathbf{r}$, and the integration of the equation of motions for the nuclei. This section discusses the numerical simulation of the equation of motion, while the determination of $U(\mathbf{r})$ is discussed in Sec. 2.3.

In this thesis, the further approximation that the nuclei follow a classical equation of motion is made, written in the Hamiltonian form:

$$\mathcal{H}(\mathbf{r},\mathbf{p}) = T(\mathbf{p}) + U(\mathbf{r}) \tag{2.13}$$

$$\mathrm{d}_t\mathbf{r} = \partial_\mathbf{p}\mathcal{H} \tag{2.14}$$

$$\mathrm{d}_t\mathbf{p} = -\partial_\mathbf{r}\mathcal{H} \tag{2.15}$$

where $\mathcal{H}$ is the so-called Hamiltonian of the system, $T(\mathbf{p}) = \sum_i \mathbf{p}_i^2/2m_i$ is the kinetic energy, and $\mathbf{p}$ is the momenta.*

Despite the simple form of Eqs. (2.13–2.15), the simulation of a microscopic system reveals important structural and dynamic properties, as demonstrated by the pioneering works of Rahman, Stillinger *et al.*,[73,74] followed by endeavours to enhance it by coupling the microscopic system to different external conditions.[75]†

2.2.1 Integration schemes

That an MD simulation yields relevant structural and dynamical information relies on its capability to visit the possible states of a system (or ergodicity). Since the equation of motion preserves the total energy of a system, one expects to visit a collection of the states of a microscopic system with constant number of particles, volume and energy (called a microcanonical or NVE ensemble). Formally, it may be shown with the Liouville equation that well-defined ensemble distribution functions follow from the symplecticity of the Hamiltonian equation of motion, from which thermodynamic quantities may be derived.[65, sec. 2.4–2.5]

This aspect is important to ensure the stability of MD simulation at a long timescale. Indeed, the principle of symplecticity and conserved quantity guides the design of integration schemes in MD simulations. In the case of NVE simulation, the velocity Verlet algorithm may be derived by Trotter factorization

---

* Such an approximation neglects the so-called nuclear quantum effects, and typically underestimates the mobility of light nuclei, to be captured by techniques like path integral MD.[72]

† Historical accounts can be found in Ref. 76, or sec. 3.7 and 4.8 of Ref. 65.

of the equation of motion,[65, sec. 3.10] in the form of a three-step procedure:

$$\mathbf{p}(\Delta t/2) = \mathbf{p}(0) - \frac{\Delta t}{2} \partial_\mathbf{r} U(\mathbf{r}(0)) \tag{2.16}$$

$$\mathbf{r}(\Delta t) = \mathbf{r}(0) + \frac{\Delta t}{m} \mathbf{p}(\Delta t/2) \tag{2.17}$$

$$\mathbf{p}(\Delta t) = \mathbf{p}(\Delta t/2) - \frac{\Delta t}{2} \partial_\mathbf{r} U(\mathbf{r}(\Delta t)) \tag{2.18}$$

It has been shown that violation of symplecticity, as is the case of popular integrators like the explicit Runge-Kutta methods, results in artefacts in simulation, such as the drift of total energy.[77, ch. 3]

A drawback of simulating the NVE ensemble is that it might not reflect a realistic dynamics of the system, which could interact with its surrounding. Systems that conceptually exchange heat with an external "thermostat" lead to an NVT (constant number of particles, volume, and temperature, or canonical) ensemble, and those interacting with an external "barostat" in addition leads to an NPT (constant number of particles, pressure, and temperature, or isothermal-isobaric) ensemble, etc.

The couplings affect the dynamic properties of interest in this thesis due to both the different statistical ensembles sampled,[78, sec. 5.3] and the changes in equation of motion along with the numerical integration scheme.[77, ch. 8] Popular approaches include the introduction of extended variables with modified conversed property, e.g. the Nosé-Hoover chains[79] or the Parrinello-Rahman barostat,[80] or the inclusion of random variables in the form of Langevin dynamics[81] or velocity rescaling.[82]

2.2.2 Finite size effects

Apart from the discretization of dynamics, the finite simulation cell and the imposed boundary condition could also systematically impact the outcome. For instance, the particle in a simulation box interacts with copies of itself under periodic boundary conditions (PBCs), leading to a systematic reduction of the self-diffusion coefficient. This effect is due to the hydrodynamic interaction of the particles with their periodic images, and can be accurately accounted for by integrating the Oseen tensor over the periodic images:

$$D_\alpha^s(L \to \infty) = D_\alpha^s(L) + \frac{\xi k_\mathrm{B} T}{6\pi\eta L} \tag{2.19}$$

where $\xi \approx 2.837$ for cubic simulation boxes, η is the shear viscosity, and L is the box size, derived from the Kirkwood-Riseman theory of polymer diffusion.[83–85]

That the finite size effect exists is not necessarily a drawback of MD simulation, a well-understood finite size effect entails knowledge on the interaction

between the simulated system with its surrounding, which underpins the validity of the simulation. The point is further exploited in Paper I.

2.3 Potential energy surface and its approximations

The above discussion paves the way to establish a relationship between the ion transport properties and the interaction between atoms, either through the theoretical framework envisioned by DHO, or computer simulations of MD. The very interaction, embedded in the potential energy surface (PES) $U(\mathbf{r})$, is the last piece of the puzzle in this thesis. Much of the interactions affecting $U(\mathbf{r})$, from the electrostatic interaction between ions central in the DHO theory, to the chemical bondings and ion-solvent interactions, finds their origin in the quantum mechanics of electrons. Here, different ways of estimating $U(\mathbf{r})$ are laid out, with the aim of studying transport properties and the emphasis on their parameterization and computational efficiency.

2.3.1 Classical force fields

The most straightforward approach to obtain $U(\mathbf{r})$ is the classical force fields describing the different types of interactions. A typical force field for molecular systems separates those into intramolecular terms, e.g., bonding, angular, dihedral, and improper, and intermolecular terms, e.g., Coulombic, and van der Waals (vdW):

$$U(\mathbf{r}) = U_{\text{intra}} + U_{\text{inter}} \tag{2.20}$$
$$= U_{\text{bond}} + U_{\text{angle}} + U_{\text{dihedral}} + U_{\text{Coul}} + U_{\text{vdW}} \tag{2.21}$$

where the individual terms are mostly "trial functions" to be fitted against experimental or theoretical data. The simple form of classical force fields grants them excellent computation efficiency: most short-range interactions can be efficiency computed and parallelized, and long-range interactions (those that decays slower than r^{-3}) may be elegantly treated by the Ewald summation[86] or its more advanced variants like the particle-particle particle-mesh Ewald summation.[87]

Despite the fact that those potentials are indeed approximate and empirical in nature, their form does reflect the most important interactions in the system. Deeper understanding of the system continues to contribute to more sophisticated and physical forms of the potential.*

---

* Exemplified by the class II force fields for hydrocarbons,[88] the glue potential for metals,[89] and the reactive force field for reactions.[90] A less recent example is the r^{-6} term of the Lennard-Jones potential,[91–93] see Ref. 94 for a historical account.

2.3.2 Density functional theory

On the other hand, $U(\mathbf{r})$ is fundamentally determined by the electronic structure, specifically the ground-state many-body electronic wavefunction given the nuclei positions under the BO approximation. Solutions to the problem deserve detailed discussion available in many textbooks.[95,96] A short path is presented here to arrive at a practical approximation, namely the Kohn-Sham density functional theory (DFT) used in this thesis.

Starting from the many-body time-independent Schrödinger equation:

$$\hat{H}_{\mathrm{elec}}\Psi_n = E_{\mathrm{elec}}\Psi_n \qquad (2.22)$$

where $\hat{H}_{\mathrm{elec}}$ is the many-body electronic hamiltonian, E_{elec} is the electronic energy, and Ψ_n is the many-body electronic wavefunction defined on the n coordinates of the electrons. The dimensionality of Ψ_n grows rapidly with n, making its solution quickly unpractical.[96] Instead, it's reasonable to factorize Ψ_n into the product of n independent one-electron wavefunctions $\chi_1, \chi_2, \ldots, \chi_n$, where the electrons only interact through a mean electric field arising from the nuclei and other electrons.

This approximation, known as the Hartree approximation, can be solved through the self-consistent field (SCF) procedure that updates the orbitals and mean field iteratively. This formalism obviously neglects the fermion nature of electrons, i.e., the exchange effect, or any correlation between the one-electron wavefunctions. The former may be accounted for by the usage of Slater determinants, known as the Hartree-Fock method, while the latter by various so-called post-Hartree-Fock methods.[95]

DFT offers a different path to treat the exchange and correlation. Instead of solving them in terms of the electronic structure, DFT states that E_{elec} is a unique functional of the ground state electron density ρ.[97] As a consequence, the energy difference between the interacting wavefunction and the non-interacting case (the exchange-correlation energy E_{xc}) is also a density functional.[98] Given the exact form of $E_{\mathrm{xc}}[\rho]$, it can be included in the SCF procedure as a potential to get the exact many-body electronic energy. Improvements to the exchange-correlation density functional have been actively developed ever since, where the systematic introduction of physics-inspired terms[99] and empirical fittings[100] are both viable. Comparison of those approximations deserves separate reviews found elsewhere.[101–103]

In contrast to alternative solutions to the electronic structure, DFT typically requires only a scaling of $\mathcal{O}\left(N^3\right)$ with respect to the system size. Together with advances in its numerical solution,[104–106] *ab initio* molecular dynamics (AIMD) based on DFT reaches the timescale of hundreds of picoseconds — sufficient to converge simple transport properties like the self-diffusion coefficients of water.[107,108] But for slower dynamics or more complex properties, further approximation as the one developed in this thesis is still needed.

2.3.3 Machine Learning Potentials

Both classical force fields and *ab initio* methods in the previous sections rely on a physics-inspired (albeit approximate) form of interatomic interactions. This section discusses yet another approach to the problem: given sufficient labels of $U(\mathbf{r})$, can one devise a most generic way to approximate it, without explicitly embedding the underlying physics?

This line of thought is by no means unique to potential building, nor is it a new subject. The study of "learning machines" dates back to the 1940s, shedding light on the capability and limits of those ML models.[109,110] The recent advance in the practical parameterization of those models revolutionized fields such as image recognition[111,112] and natural language processing.[113]

The building of a ML potential has much in common with that of a classical FF, but by casting it as a regression problem, we see it from the two different perspectives: the representation of $U(\mathbf{r})$ with a small set of constraints imposed by physics, and the sampling of sufficient configurations to parameterize it.

The first problem is greatly simplified with the assumption that $U(\mathbf{r})$ can be further approximated as a sum of contributions from each atom i depending on its neighbourhood.[50]* In addition, it is advisable to use a description of the neighbourhood that is invariant to symmetry operations such as translation, permutation and rotation (invariance).[50,114,115] Finally, the descriptor should be expressive enough to distinguish any distinct structures (completeness).[115–117]

Those principles guide the design of various local descriptors, leading to much better understanding about their limitations and connections in the past decade. Paper V discussed one of those designs in more detail. As a result, those methods do provide a middle ground between classical force fields and *ab initio* methods, with which simulations at DFT accuracy reaches the nanosecond timescale necessary for elucidating transport phenomena involving chemical reactions, as is demonstrated in Paper IV and Paper VII.

On the other hand, the performance of machine learning potentials (MLPs) (like other ML models) typically relies on the high-dimensional description. This implies the difficulty in both determining the growing number of parameters and building a representative dataset (known as the curse of dimensionality). In contrast to the promising performance of ML models, understanding about their transferability is far from satisfactory. For MLPs, this manifests as the difficulty of gauging the performance of MLPs prior to their usage.[118] An example for this is discussed in Paper VI, and the practical remedy with the adaptive on-the-fly learning scheme is discussed is Paper VII, among many other attempts to construct reliable workflows for building MLPs.[119–122]

---

* This signifies the locality of interactions. While reasonable, especially when dealing with $U(\mathbf{r})$ in the bulk system, it could have significant implications when long-range interactions play their role. Validation and extension of the present scheme still take physical insights.

3. Understanding Transport Coefficients in Electrolytes

A common question in the study of transport coefficients is how they differ from the *ideal* behaviour, i.e. how Eq. (2.5) deviates from Eq. (2.4). Working with MD simulation, one expects to capture both exactly, given an accurate $U(\mathbf{r})$. Classical force fields in the form of Eq. (2.20) is used in this chapter, as no chemical reactions are expected in the studied systems. Before proceeding, a few more transport coefficients are needed to represent the non-ideality. With the Nernst-Einstein (N-E) relation, one gets the ideal ionic conductivity:

$$\sigma_{N-E} = \frac{1}{k_B T} \sum_\alpha q_\alpha^2 \rho_\alpha D_\alpha^s \qquad (3.1)$$

where ρ_α is the number density of α, while the Green-Kubo (G-K) relation relates the conductivity to the displacement of the itinerant polarization $\mathbf{P}(t)$:

$$\sigma_{G-K} = \lim_{t \to \infty} \frac{V}{6k_B T t} \left\langle \|\Delta\mathbf{P}(t)\|^2 \right\rangle \qquad (3.2)$$

The so-called distinct conductivity represents the non-ideality due to each pair of species in the case of 1:1 binary electrolytes:

$$\sigma_{\alpha\beta}^d = \lim_{t \to \infty} \frac{q_\alpha q_\beta (2 - \delta_{\alpha\beta})}{6k_B T V t} \left\langle \sum_{i \in \alpha} \sum_{j \in \beta, j \neq i} \Delta\mathbf{r}_i(t) \cdot \Delta\mathbf{r}_j(t) \right\rangle \qquad (3.3)$$

It's easy to show that σ_{G-K} indeed is equivalent with Eq. (2.7), and that $\sigma_{\alpha\beta}^d$ captures all the ion-ion correlations that contribute to the difference between σ_{G-K} and σ_{N-E}. Experimentally, σ_{N-E} can be determined through isotopic tracers or PFG-NMR, while σ_{G-K} is the ionic conductivity in standard impedance measurements.

Given the availability of those measurements, they are often used to get the so-called "ionicity" (or its inverse, known as the Haven ratio) that connotes the "dissociation degree" in the Arrhenius picture.[123] Recalling Eq. (2.12), one shall note that the electrophoretic effect also manifests as a form of correlation (and relaxation is at least partially captured by σ_{N-E}).

The simulated transport coefficients are compared to experimental values for two purposes: to see whether the model $U(\mathbf{r})$ captures the essential interactions, and to find out which of the microscopic picture (association or electrophoretic) dominates the ion-ion correlations.

3.1 Paper I: the role of viscosity

3.1.1 Finite size effect

As a proof of principle, Paper I considers two typical electrolytes, the aqueous solution of sodium chloride (NaCl/aq) and the ionic liquid (IL) [BMIM][PF$_6$]. Knowing that finite-size effect exists for self-diffusion coefficients (and thus σ_{N-E}), we first examine if it affects σ_{G-K} as well.

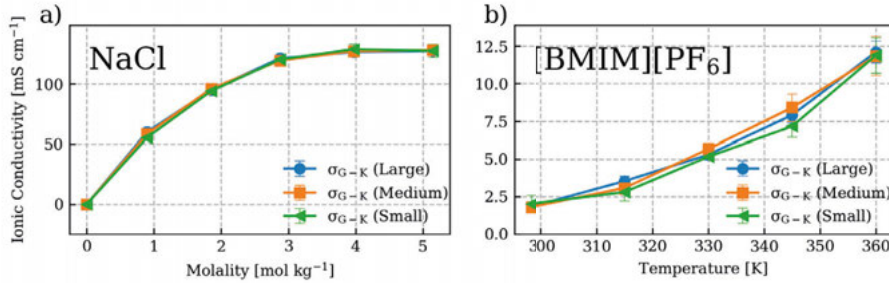*Figure 3.1.* σ_{G-K} with different sizes of simulation box for (a) NaCl/aq at 20 °C and different concentrations, and (b) [BMIM][PF$_6$] at different temperatures. Adapted from Paper I under a CC-BY license.

As shown in Fig. 3.1, σ_{G-K} shows almost no size dependency. Such absence of finite size effect was reported for the viscosity,[85] and one may reconcile the observation as both properties depend on the time-correlations of collective quantities of the entire simulation box, so that the self-interaction in these cases might be eliminated by the boundary condition.
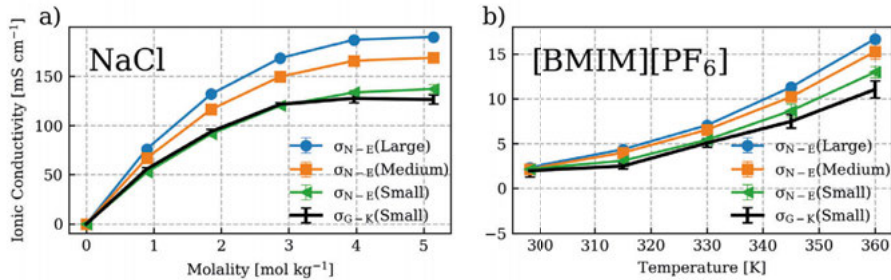
3.1.2 Crossover box size

Figure 3.2. σ_{N-E} with different box sizes for (a) NaCl/aq at 20 °C and different concentrations, and (b) [BMIM][PF$_6$] at different temperatures. σ_{G-K} with the small box is plotted as a reference. Adapted from Paper I under a CC-BY license.

When comparing σ_{N-E} and σ_{G-K} at different box sizes, an interesting observation is that the two conductivities overlap at the smallest box size (L_{min}),

as shown in Fig. 3.2. Given the finite size effect of self diffusion in Eq. (2.19), one would expect a simple inverse relation between the specific conductivity and viscosity, in which $L_{\min}$ is a system-specific length scale:

$$\lim_{L \to \infty} (\Lambda_{N-E} - \Lambda_{G-K}) \cdot \eta \approx \frac{2 N_A q^2 \xi}{6 \pi L_{\min}} \tag{3.4}$$

Inspired by this observation, we took experimental data to verify if the rule hold for general cases, where the Λ_{N-E} corresponds to that derived from the self-diffusion coefficient measured with PFG-NMR (Λ_{NMR}), and Λ_{G-K} to that with impedance measurements (Λ_{Imp}).
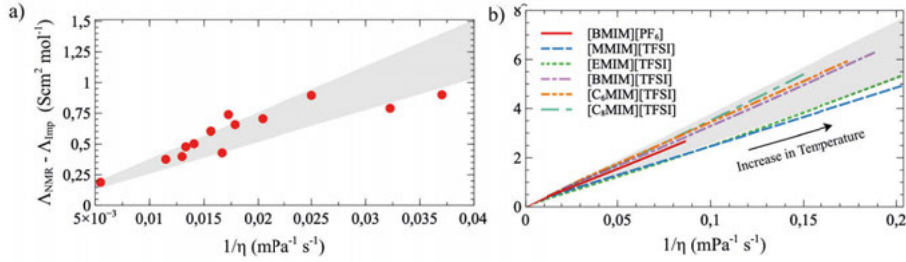

Figure 3.3. Experimentally measured deviation of ionic conductivity for (a) 13 types of ILs extracted from Ref. 124, and (b) 6 types of ILs at various temperatures using fitting coefficients of Vogel-Fulcher-Tammann equations from Ref. 125 and 126. The theoretical bounds set by the MD simulations of NaCl/aq and [BMIM][PF$_6$] using Eq. (3.4) are shown as grey areas. Adapted from Paper I under a CC-BY license.

As shown in Fig. 3.3, the linear relation between the deviation and viscosity holds well as a rule of thumb to estimate the contribution of ion-ion correlation of ionic conductivity. According to the trend of $L_{\min}$ in Fig. 3.3 (b), $L_{\min}$ seem to decrease with larger cations, which might relate to the electrostatic interaction between ions.

The strong correlation with viscosity, especially within a single IL, seems to suggest the significance of hydrodynamic interaction or the electrophoretic effect. On the other hand, the fact that two conductivities coincides puts doubt on whether kinetically stable ion pairs exist in those electrolytes.

3.2 Paper II: the role of ion-pair lifetime

3.2.1 Lifetime of ion pairs

Following the previous work, Paper II aims to clarify the concept of ion pairing by making the distinction between the long-lived ion pairs and those that exist as transient structures. In a previous publication,[127] it is shown that the solvent polarity, tuned by the atomic charges in the MD simulation, determines the coordination patterns and transport mechanism in the polymer electrolyte

PEO-LiTFSI. The result is used in this paper to get a series of electrolytes with different ion-pair lifetimes (τ_{+-}), defined using the stable-state picture (SSP) proposed by Laage and Hynes.[128]
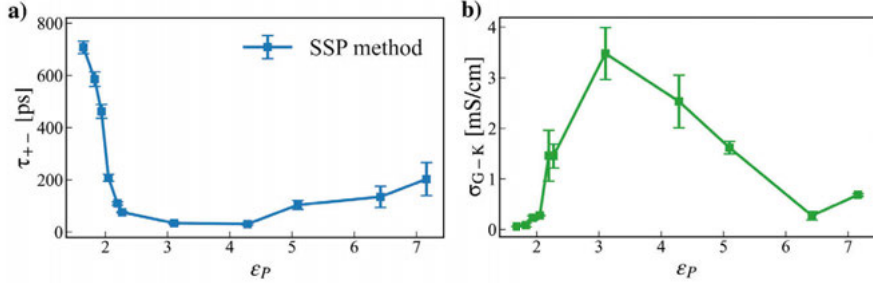

Figure 3.4. (a) The ion-pair lifetime τ_{+-} as a function of ε_P; (b) the Green-Kubo conductivity σ_{G-K} as a function of ε_P. Adapted from Paper II under a CC-BY license.

As shown in Fig. 3.4, the solvent polarity ε_P does induce a change of conductivity in both the high- and the low-ε_P limit. In both cases, the ionic conductivity decreases with the ion-pair lifetime, which appears to support the view that ion pairs reduce the ionic conductivity through their positive correlation, which is more significant at high τ_{+-}. We could nevertheless envision an alternative explanation of the correlation that both τ_{+-} and σ_{G-K} reflects the overall mobility of the system. In this case, we shall expect all correlation functions to decay with viscosity in the same way, i.e., less significant at high τ_{+-}.

3.2.2 Two regimes of ion pairing

The two patterns of correlation both happen in the simulation, where positive ion-ion correlation (negative σ_{+-}^d) is observed at low ε_P, and vice versa. As shown in Fig. 3.5, the two regimes can be qualitatively described by two asymptotic curves: for the long-lived regime, σ_{+-}^d scales linearly with τ_{+-} as a proxy to the ion-pair population, and for the short-lived regime, it scales with $1/\tau_{+-}$ as indication of mobility.

The results showcase how the ion-ion correlation provides a comprehensive picture of the microscopic dynamics of electrolytes, which complements what can be inferred from σ_{G-K} or τ_{+-}. Paper III demonstrates how the transport coefficients measured experimentally corresponds to the ion-ion correlations discussed so far, to establish the link between experiment and simulations.
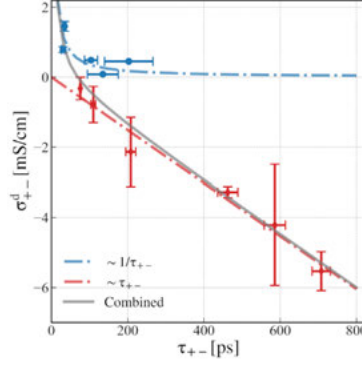
Figure 3.5. Scaling of σ^{d}_{+-} with the ion-pair lifetime τ_{+-} at different solvent polarity strengths. A clear separation of trends is seen between the red regime ($\varepsilon_{\mathrm{P}} < 3$) and the blue regime ($\varepsilon_{\mathrm{P}} > 3$); each trend is represented by a linear or inverse fit, and the sum is shown as the grey line. Adapted from Paper II under a CC-BY license.

3.3 Paper III: the role of reference frame

3.3.1 Negative transference number

The ion-ion correlations discussed so far have significant impacts on the operation of electrochemical devices. Since only the working ions are consumed during the steady operation of the cell, a concentration gradient builds up in the bulk, leading to internal resistance or even salt depletion.[14] The transference number t_α, defined as the fraction of migrational currents carried by α, determines the concentration gradient,* and it naturally raises concern when negative and even contradicting values of t_+ (for Li$^+$) were reported.[130,131]

The observation of the negative transference number may partially be reconciled, by noticing that t_α, unlike σ, dependents on the RF. In a binary salt solution, t_+ may be converted to the desired RF given the correct weight factor, i.e., to convert between barycentric RF (denoted as M) and the solvent-fixed RF (denoted as 0) for the PEO-LiTFSI system, given the weight fractions ω_α:

$$\omega_0 t^0_+ = t^{\mathrm{M}}_+ - \omega_- \tag{3.5}$$

With such a conversion, it's already clear that the experimentally measured[130] negative t_+ can be reproduced from simulation. As shown in Fig. 3.6. The force fields used in Paper II seem to reproduce the measurements reasonably well. We nevertheless proceed to derive the complete set of Onsager coefficients from experimental data using Eqs. (2.7–2.9), to fully evaluate the PES, and to understand the interpretation of ion-ion correlations.

---

* The term transference number is often used interchangeably with the transport number.[129] They are nevertheless distinct definitions, as suggested in Refs. 31 and 14, when ions are categorized by aggregates. The former refers to the net currents of one ionic species, while the later refers to individual contributions from different aggregates. As the former is what is measured both in experimental studies[130,131] and in the present thesis, it is used throughout.
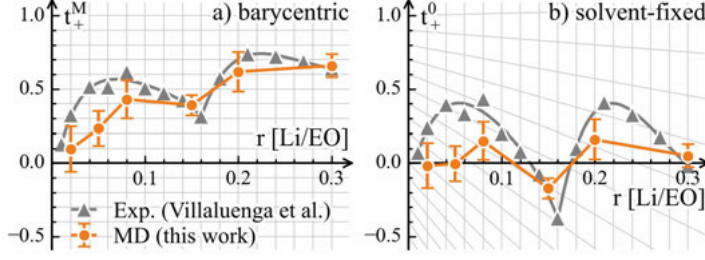
Figure 3.6. Transference numbers under (a) barycentric RF and (b) solvent-fixed RF in PEO-LiTFSI at different concentrations, the conversion if performed with Eq. (3.5), the experimental data is taken from Ref. 132 and the conversion rule is presented as a projection of gridlines. Adapted from Paper III under a CC-BY license.

3.3.2 Reference frame and ion correlation

Conversion between Onsager coefficients is not trivial, as is discussed in Ref. 133, the conversion should follow the constraint of conserving the entropy production, and between a set of independent fluxes and driving forces.
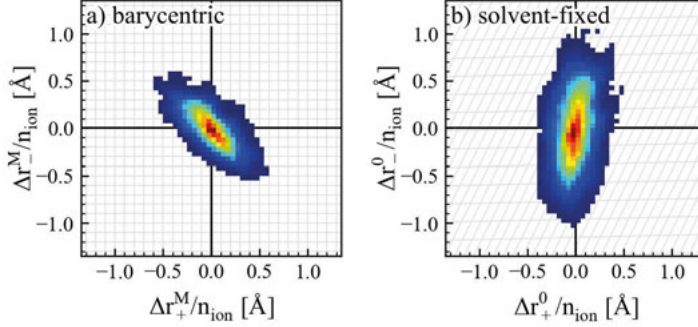

Figure 3.7. Transformation of the normalized displacement correlations between (a) the barycentric RF and (b) the solvent-fixed RF. The displacements are normalized by the number of ions. The conversion rule is presented as a projection of grid lines. Adapted from Paper III under a CC-BY license.

The conversion rule might be better understood considering the connection between Onsager coefficients and the displacement correlation functions in Eq. (2.9), as shown in Fig. 3.7, when both displacements undergo an RF transformation, a change of sign might occur in the correlation.

Upon proper RF transformation, we again see an agreement between simulation and experiments for all the Onsager coefficients. Specifically, at the point where the negative t_+^0 is observed, the correlation between cation and anion is actually positive in the barycentric RF, unlike the case of long-lived ion pairs in Paper II. This suggests that the negative transference number is
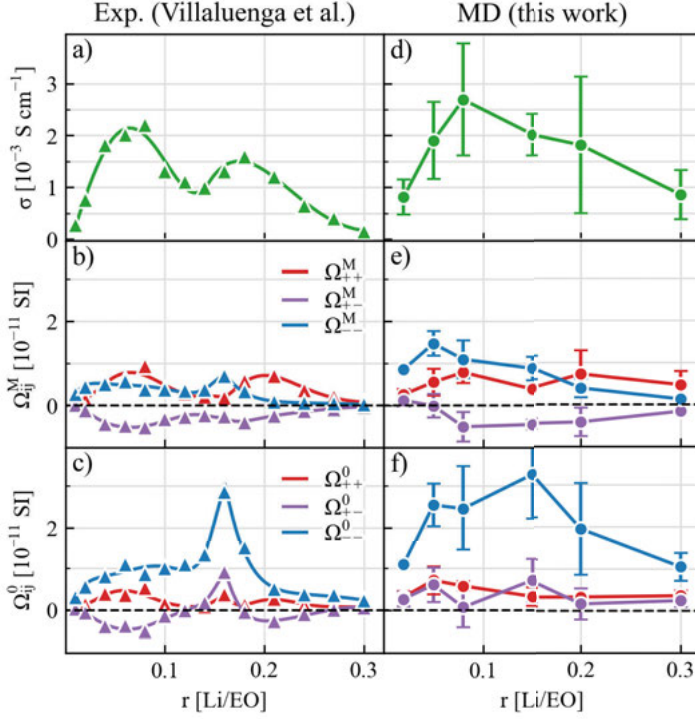
27

Figure 3.8. Ionic conductivity and Onsager coefficients under the barycentric and solvent-fixed RF derived from (a-c) experimental measurements in Ref. 132 and (d-f) MD simulations. Adapted from Paper III under a CC-BY license.

more of the effect of the chosen RF rather than an indication of ion association.

3.4 Summary

To summarize the results, the electrophoretic interaction of a hydrodynamic origin seems to play a ubiquitous role in the ion-ion correlations in electrolytes, while for the studied systems, not much sign of ion pairing is gathered. The simulation with the classical force fields generally gives reasonable predictions when compared to experiments. Though, the agreement could only be qualitative (e.g. Fig. 3.8). Despite limited precision, the microscopic view does elucidate the experimental observations, exemplified by the more crisp distinction between long- and short-lived pairs and the revelations of the RF dependence of Onsager coefficients.

4. Developing Neural Network Potentials for Liquid Electrolytes

In exploring electrolyte materials, a particularly interesting class is the proton-conducting materials,[18] which find applications in electrochemical cells such as the Ni−Cd batteries, and fuel cells. Such materials are also relevant for biological processes, e.g., ion transport through cell membranes. There, the high mobility of the proton is explained by its structural diffusion via the Grotthuss mechanism.[134] The concerted proton transfer (PT) along a chain of hydrogen bonds (HBs) conceptually allows for the fast transport of ions, as illustrated below in Fig. 4.1.
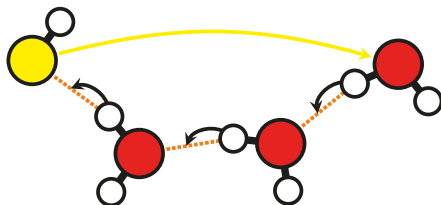

Figure 4.1. An illustration of the conduction of a hydroxyl ion (OH⁻) via a Grotthuss-type PT. The hydroxyl ion and its motion are highlighted in yellow, and the hydrogen bonds are highlighted in orange.

Simulating those proton conducting materials requires $U(\mathbf{r})$ that can deal with reactions, either through electronic structure calculations, or force fields based on knowledge of the reactant and product states, exemplified by the empirical valence bond approach,[135,136] or reactive force fields.[137] The former (producing dynamics at the scale of tens of picoseconds) suffices to converge the self-diffusion in small systems,[46] but falls short when higher concentration or slower dynamics is of interest. The latter could reach the scale of nanoseconds, but its parameterization requires prior knowledge about the reactions.

A third way exists, as mentioned in Sec. 2.3.3, by constructing ML models of $U(\mathbf{r})$ (i.e. MLPs) directly from *ab initio* data. Specifically, we focus on a class of MLPs based on neural networks, or NNPs. The goal of this chapter is clear: one aims to reach the timescale necessary to determine the transport coefficients and reproduce the dynamics specified by the underlying electronic structure calculations as much as possible.

4.1 Paper IV: ionic conductivity in NaOH/aq

4.1.1 The proton transfer contribution

As a first attempt of using NNPs for the modelling of transport properties, we take the classical proton conducting system — aqueous solutions of sodium hydroxide, where a NNP has been developed and tested.[138]

The first difficulty of computing the transport coefficients with PT, is the definition of OH$^-$ during the simulation. Due to the possible Grotthuss-type PT, we need to identify the anions by the connectivity of atoms; to compute the time correlation functions as Eq. (2.3), we also need to track their identity, where we applied the "Hungarian algorithm".[139]
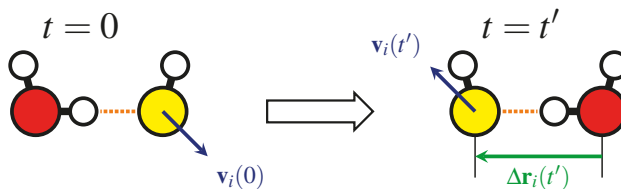

Figure 4.2. An illustration of the velocities and displacement of the hydroxyl ion in the present definition, before and after a PT event.

With that, each anion will have defined positions and velocities at each time step. As illustrated in Fig. 4.2, the time correlation based on the positions takes into account the displacement of PT, while that based on the velocity correlation function (VCF) only describes the drift of the ion:

$$D_\alpha^s = \frac{1}{3N_\alpha} \int_0^\infty dt \sum_{i \in \alpha} \langle \mathbf{v}_i(0) \cdot \mathbf{v}_i(t) \rangle \tag{4.1}$$

Comparing the self-diffusion coefficients computed with the two methods, the role of PT is evident in the self-diffusion coefficient. As shown in Fig. 4.3 (a,b), the D^s of OH$^-$ is significantly boosted in most cases, while that of Na$^+$ is not. On the other hand, the correlation between ions in Fig. 4.3 (c,d) shows no significant difference between the VCF and MSD values, indicating a weak correlation between PT and other motions of ions.

4.1.2 Ionic conductivity and non-ideality

The ionic conductivity σ is compared against experimental measurements at different temperatures (Fig. 4.4 a), where a good agreement is observed, especially at ambient temperature (293 K). The result is encouraging, as the potential is derived from DFT calculations only. Like what is discussed in Papers I-II, deviation of σ_{G-K} from σ_{N-E} decreases with the lifetime of Na$-$OH$^-$ pairs or its coordination number (Fig. 4.4 b), as another indication that hydrodynamic interaction rather than ion pairing is the source of non-ideality in the case of NaOH/aq.
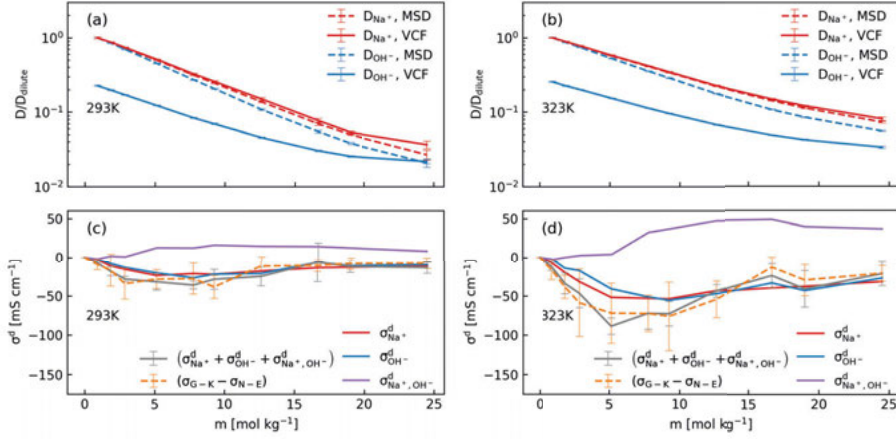
Figure 4.3. (a,b) Scaled self-diffusion coefficients $D^{\text{s}}/D^{\text{s}}_{\text{dilute}}$ for Na^+ and OH^-; (c,d) distinct conductivities σ^{d} for NaOH/aq at two different temperatures (293 K and 323 K). All the VCF (solid lines) and MSD (dashed lines) values were reported in the case of D^{s}, while for σ^{d}, only the net contribution was reported for the MSD values. Adapted from Paper IV under a CC-BY license.

4.2 Paper V: a generic atomic neural network library

4.2.1 The PiNet architecture

The previous work uses the Behler-Parrinello Neural Network (BPNN) architecture, as illustrated in Fig. 4.5. As discussed in Sec. 2.3.3, it features a decomposition of the total energy into atomic environment-dependent energies. Having demonstrated the power of this approach, one notices that descriptors of the atomic environment needs to be handcrafted for the specific system before the parameters in the feed-forward NN (yellow nodes in the Fig. 4.5) can be determined.
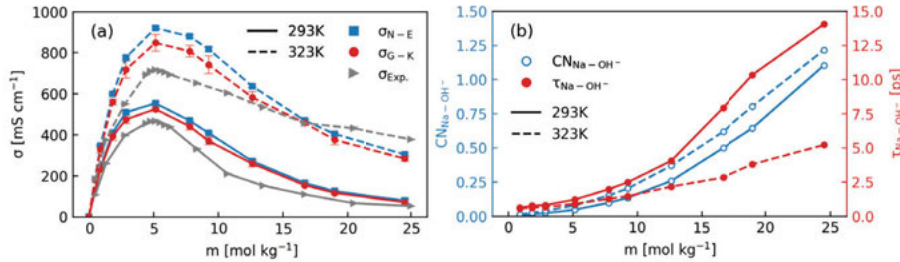

Figure 4.4. (a) Concentration-dependent ionic conductivities ($\sigma_{\text{N}-\text{E}}$ and $\sigma_{\text{G}-\text{K}}$) computed from MD simulations and those measured in experiments at 293 K and 323 K; (b) coordination numbers and residence time of Na^+-OH^- pairs. Adapted from Paper IV under a CC-BY license.
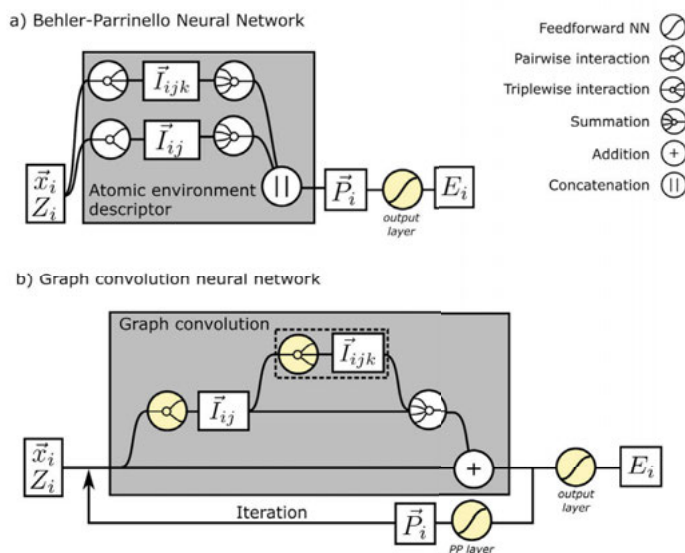
Figure 4.5. Illustration of (a) the BPNN and (b) the PiNet architecture. Adapted from Paper V under a CC-BY license.

Paper V takes a different route by designing a neural network that builds up the features from the feed-forward NN. This method of building NNs that iteratively updates node (or atomic properties, denoted as $\vec{P}$) and edge features (or pairwise/triplets interactions, denoted as $\vec{I}$) of a graph structure is also known as graph convolution (GC) NNs or message passing (MP) NNs.
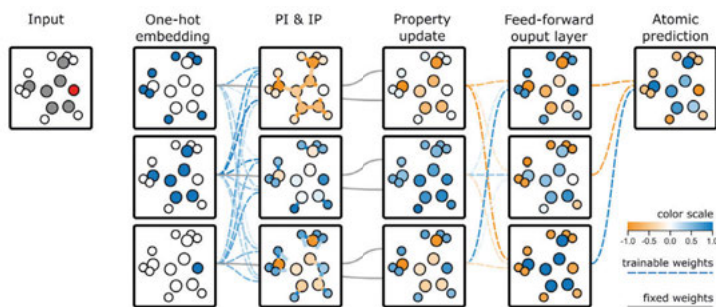
Figure 4.6. Visualization of the PiNet architecture, where the atoms and bonds in each box indicate normalized activations of the atomic property and pairwise interaction, respectively. Dashed lines show the normalized trainable weights. Adapted from Paper V under a CC-BY license.

The difference between PiNet, and related works such as SchNet,[140] is the form of their pairwise interaction. This architecture was designed to mimic the chemical intuition in the latent representation inside a neural network

(NN). As demonstrated in Fig. 4.6, the latent variables of PiNet focus on the short-ranged pairwise interactions, as expected by chemical intuition. In a later work, those edge features are found useful in constructing the response properties of molecules and materials, where the interpretation of such short-ranged pairwise interactions as physical quantities becomes the determining factor.[141]

4.2.2 Performance of PiNet

The performance of PiNet is benchmarked against a number of publicly available datasets, from small molecules to perovskites to the aforementioned NaOH/aq system, as shown in Fig. 4.7. State-of-the-art results were obtained, and a steady decrease in error with respect to training data size is found, indicating sufficient flexibility or completeness of the PiNet architecture.
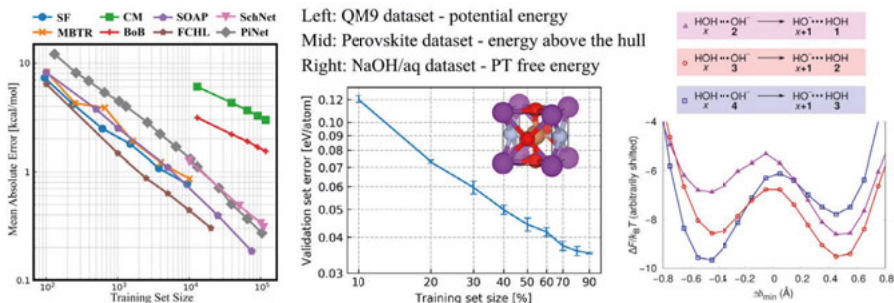

Figure 4.7. Performance of the PiNet architecture, left: the total energy for small molecules against the QM9 dataset,[142] adapted from Ref. 11 under a CC-BY license. Mid: energy above the hull for perovskites,[143] and right: PT free energy profile from MD simulations in Paper V, adapted from Paper V under a CC-BY license. See original articles for details about the training and evaluation procedure.

4.3 Paper VI: training algorithm and model performance

4.3.1 Impact of training algorithm

The BPNN, as a reference NNP architecture for atomistic simulation, was also implemented in PiNN. During the benchmark of the PiNN code, it was noticed that when training the same BPNN on a water dataset labelled at the BLYP level of theory,[144] additional data is needed to get a stable potential for both NVT and NPT simulations. The case is studied in detail in this work, first by noticing that a different training algorithm, namely the extended Kalman filter (EKF), was used in the original implementation of BPNN in the RuN-Ner code.[145] To pinpoint what has affected the performance of BPNN, the

same algorithm was implemented in PiNN, to test it against the popular Adam optimizer[146] with the same set of force and energy labels and implementation details.
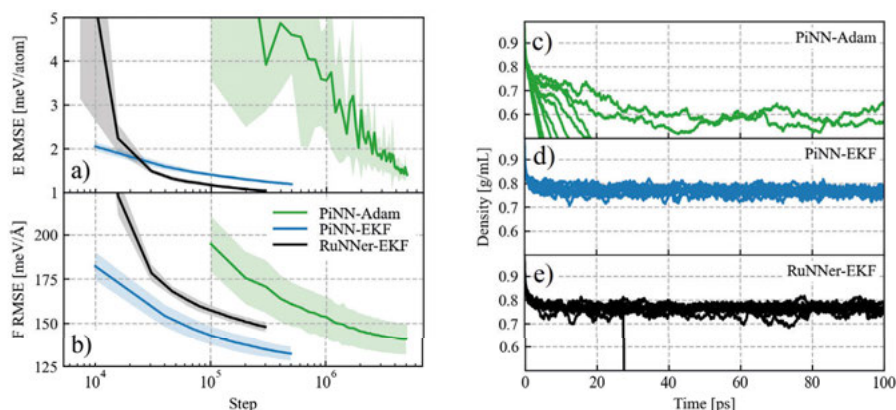

Figure 4.8. (a,b) Evaluation error metrics during training and (c-e) density evolution during NPT simulation for different implementations of BPNN trained with the BLYP dataset. 10 instances of each setup are trained, their standard deviations are shown as shaded areas in (a,b), and the density evolutions are plotted individually in (c-e). Adapted from Paper VI under a CC-BY license.

As shown in Fig. 4.8 (a), despite minor differences, the EKF implemented in PiNN has a similar convergence as the RuNNer implementation, approximately 10 times faster compared to Adam.* Both of the EKF implementations produce models that give reasonable NPT simulations with a stable density. In stark contrast, all models trained with the Adam optimizer predicts unstable NPT trajectories towards a low density. Although the force and energy error metrics indicate a similar accuracy in the Adam and EKF models.

The result is strong evidence that the training algorithm affects the stability of the potential, and since the error metrics are close, it reflects a difference in the transferability of the model. This is further validated by experimenting on another dataset of water constructed at the RPBE-D3 level of theory to sample a broad distribution of configurations,[149] where the density prediction becomes less sensitive to the training algorithm, as shown in Fig. 4.9. This means that the difference can be mitigated with a better-constructed dataset.

4.3.2 Information geometry of NNPs

Both Adam and EKF minimize the loss function given a stochastic signal of the gradient of the loss function, a high dimensional and non-convex surface

---

* Unfortunately, this is accompanied by a higher computational cost per step and memory cost. More efficient implementations of second-order optimizers such as EKF are actively developed in the ML community.[147,148]
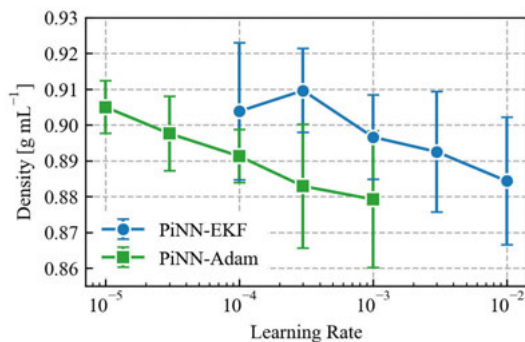
Figure 4.9. Density prediction with different training algorithms and training rates with the RPBE-D3 dataset. Adapted from Paper VI under a CC-BY license.

that resembles the PES. That different algorithms get qualitatively different models means they favour local minima of the loss function with different characteristics; similar observations were made in the ML community, though a universal metric for "good" minima was known.[150,151] As the algorithms use the Fisher information matrix $\mathcal{I}$ (an information geometric metric characterizing the local curvature) or its approximation to rescale the optimization direction, we investigated whether the final models can be differentiated by $\mathcal{I}$. As shown in Fig. 4.10, the more robust models tend to have a higher distribution of eigenvalues (or locally sharper).

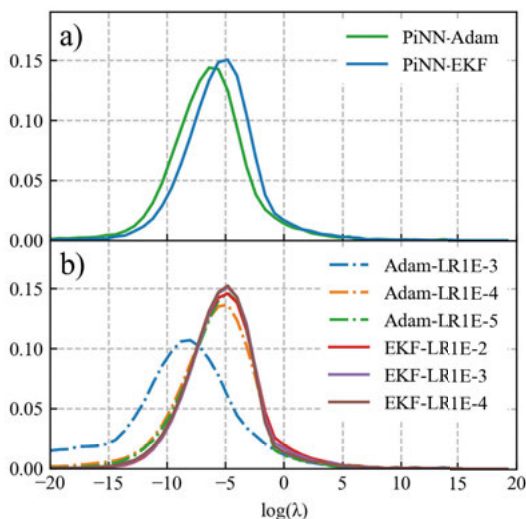*Figure 4.10.* Distributions of eigenvalues λ of the Fisher information matrix for the models trained on (a) BLYP dataset and (b) RPBE-D3 dataset. Note that the logarithm scale of λ is used. Adapted from Paper VI under a CC-BY license.

4.4 Paper VII: an adaptive learn-on-the-fly workflow

4.4.1 Devising an adaptive learn-on-the-fly workflow

Paper VI highlights the procedure of parameterization as an important factor contributing to the high performance of NNPs. The effect is not fully revealed by typical error metrics as root mean squared error (RMSE), but nevertheless manifests itself in the long timescale dynamics. This reflects one shortcoming of NNPs that they can only be tested on a small fraction of the configurations, typically sampled with *ab initio* methods. In lieu of a "golden" NNP with perfect transferability, a more practical alternative is to continuously improve the model when it samples larger volumes in the configuration space, either with a prescribed pace (learn-on-the-fly, or LOTF), or with an uncertainty estimation of the model (active learning, or AL).

Figure 4.11. Workflow for one generation of the adaptive LOTF. Green boxes denote processes, red boxes denote data which are updated at each iteration, and blue boxes denote loops and decisions.

The AL approach has its advantage, as the uncertainty estimation helps to reduce the number of labels needed. Such estimation, however, requires calibration to the actual error, and the correlation is not always ideal. To achieve the extension of timescale with the best possible estimation of error, an adaptive LOTF workflow is devised, where, instead of biasing the distribution of data to be labelled, the labelling frequency of a LOTF workflow is adaptively chosen based on past testing results. An illustration of the workflow is in Fig. 4.11.

To test the workflow, we opted for the PIL system $[C_1IM][HOAc]$, where ions form upon PT between the Brønsted acid/base pairs. Like NaOH/aq, the Grotthuss-type PT is conjectured for this system. Previous AIMD calculations reports the existence of PT,[47] but the simulation time is too short to quantify the diffusion coefficient in the diffusion regime. The system serves as a stringent test of the methodology, given the scarce prior knowledge available.
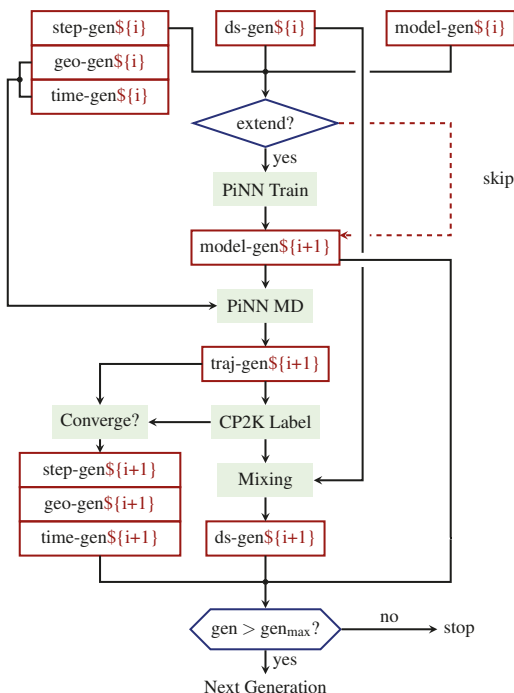
4.4.2 Adaptive LOTF of [C$_1$IM][HOAc]

One instance of the adaptive LOTF procedure is shown in Fig. 4.12 (a-c), the PiNet architecture developed in Paper V is applied here. As expected, the initial model generated from short AIMD trajectories does not give a stable model, as indicated by the high test error computed on the sampled trajectory, comparing to the evaluation error computed on the randomly split validation set. With the adaptive LOTF procedure, the model becomes more stable over generations, as indicated by the diminishing spikes in the test set error and the sampling timescale increases accordingly.
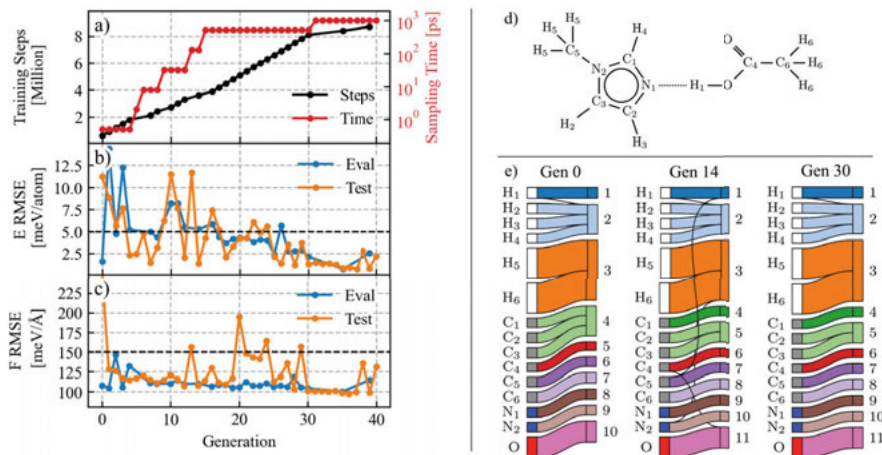

Figure 4.12. Evolution of a NNP during the adaptive LOTF process. (a) total training steps and the sampling timescale; (b,c) energy and force RMSE; (d) manual assignment of the atomic types; (e) correlation between the latent space structure of the model and manually assigned labels.

We also monitored the change of latent space structure to better understand the evolution of the model. This is achieved by performing a clustering of the atomic features in the latent space, and comparing them to manually labelled atomic types. As shown in Fig. 4.12 (d,e), the first generation of the model already formed a reasonable description of atoms of different types. During the adaptive learning process, the two chemically distinct carbons were further separated into two clusters. Interestingly, in between the training process, some spurious links appear between the two assignments, indicating certain miscategorised atoms.

That the cluster structure of the latent space can reveal interpretable information about atoms is encouraging. The present algorithm depends only on a distance metric in the latent space, meaning it can be applied to most of the present MLP architectures, providing a means to compare models regardless of their implementation. The change of latent space during the adaptive LOTF also opens the opportunity of using the structure to guide the sampling.

4.4.3 Long timescale dynamics of [C$_1$IM][HOAc]

To validate the model, we first compare the structure of the PIL in terms of the radial distribution functions. As shown in Fig. 4.11 (a), the radial distribution functions of the PiNN model agrees well with the reference calculations performed with the CP2K[105] code for the initial relaxation (PiNN 100 ps and CP2K 100 ps) from configurations relaxed with a classical MD code. Notably, the structure underwent significant change after a long relaxation with PiNN (5 ns), this is further validated with an extra CP2K reference calculation for 100 ps, starting from the configuration relaxed with PiNN, named as CP2K 100 ps (II). The relaxation seems to diminish the HB network over a long period, where a change of the HB structure towards that dominated by acid-base pairs is observed, as shown in Fig. 4.13.
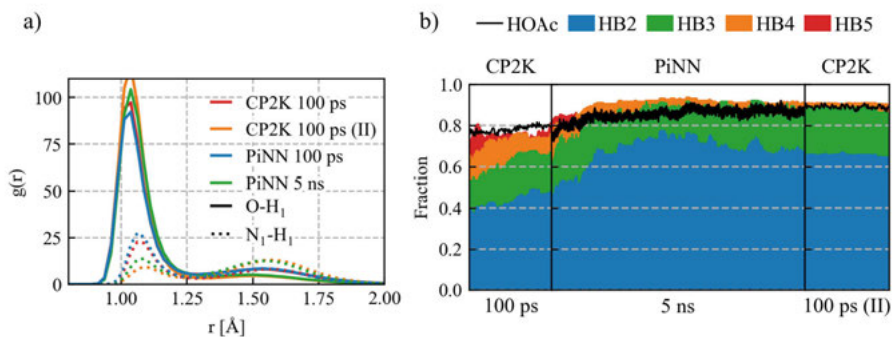

Figure 4.13. Structural relaxation of [C$_1$IM][HOAc] during the simulation (a) radial distribution functions between the active hydrogen (H$_1$) and nitrogen (N$_1$) or oxygen (O); (b) the size of hydrogen-bonded networks during the simulation shown as stacked filled regions, and the fraction of molecular species shown as black lines.

The significant change in HB structure raises the question of how the formation of acid-base pairs changes the dynamic properties of the PIL. The lifetime of such pairs is first examined, and it seems much longer than that of the covalent bonds formed by H$_1$, as shown in Fig. 4.14 (a). This suggests a microscopic picture of long-lived acid-base pairs, while the active proton oscillates at a shorter timescale such that the pair switches from and to an ionic state frequently.

We then proceeded to see how the slow relaxation affects the transport properties, starting from the self-diffusion coefficients of H$_1$. It is clearly shown in Fig. 4.14 (b) that the MSD of H$_1$ does not reach the diffusion regime at a picosecond scale and that the mobility is significantly lower than a short-timescale estimation. Unfortunately, the observed diffusion coefficient is much lower than the experimental measurements. Since the time correlation agrees well at a short timescale, the most viable explanation is that the underlying DFT approximation does not predict a correct melting point of [C$_1$IM][HOAc],
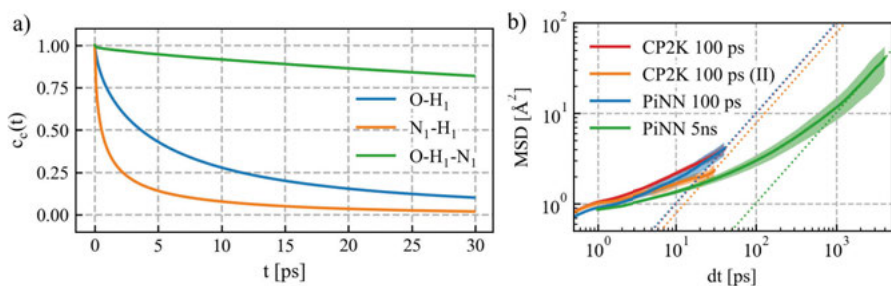
Figure 4.14. Dynamic properties of [C_1IM][HOAc] during the simulation (a) the life-time of chemical bonds formed by H_1, and the hydrogen-bonded dimeric configuration $O-H_1-N_1$; (b) MSD of the active proton in different simulations.

so that a higher temperature or another DFT functional is needed to be able to compare to room temperature experiments, as has been observed for water earlier.[152]

4.5 Summary

This chapter demonstrates the power and pitfalls of NNPs in the simulation of electrolyte materials. As a tool to bridge electronic structure calculations and the dynamics of nuclei, it fulfils the demand well. This is demonstrated by the simulation of NaOH/aq, and reaches quantitatively correct predictions of the phenomenological coefficients.

On the other hand, as "learning machines", NNP bears the great complexity coming from its great ambition. As demonstrated in Papers V-VII, factors include at least the architecture of the model, its parameterization procedure and the coupling with the sampling procedure. During the method development in this chapter, a number of empirical observations are made, though much more insight is still demanded to understand how and why those models work.

5. Concluding remarks

To sum up, the present thesis takes a deep dive into the simple phenomenon of: $\mathbf{J}_\alpha = \sum_i \Omega_{\alpha\beta} \mathbf{X}_\beta$ — a linear flux response in a system given several driving forces. This simple relation characterizes ion transport in electrolytes, as the defining properties of electrolytes in electrochemical devices.

With the atomistic simulations used throughout the thesis, the goal has been, above all, to establish a connection between the microscopic picture of electrolytes as ion-containing materials to a mesoscale one as an ion-conducting matter. The simulation has not been used as a means to bypass or overwrite the established conceptual frameworks (from Arrhenius' to Onsager's) but rather as computer experiments to demonstrate those principles.

This starts from the realization in Paper I and Paper IV, that the ion correlations largely arise from hydrodynamics in commonly seen electrolytes. And it is followed by the identification of a transition of ion dynamics from one governed by the Arrhenius-type ion association, to that by the DHO-type electrophoretic effect (Paper II). Apparently, such an identification is instructive to correctly interpret experimental data, a point that is stressed in Paper III, where some of the puzzles in the literature find their origin in the fundamental constraints set by the law of irreversible thermodynamics.

In doing so, the demonstrative rather than the predictive power of modelling is emphasized in the first part of the thesis. Though the two cannot really be separated, as prediction will not be possible without solid conceptual links, inaccurate models will not be relevant to understand real-world processes. The second part of the thesis indeed focuses on predictive models with the aim of getting an *ab-initio*-level of accuracy in long MD simulations, given the difficulty of attaining such force fields for reactive systems.

Instead of building the models on a chemical or physical ground, a data-driven approach is taken, where we focus on the interplay between representation, data, and the parameterization process. Leveraging the advances in computational power and generic regression methods, this approach succeeded in putting extra phenomena into the grasp of atomistic modelling and providing more stringent tests for the approximated exchange-correlation functionals in density functional theory (Paper IV and Paper VII).

Like other disciplines of science, the development of ML methods stems from the entwined fortuitous observations and theoretical consolidations. During the development of methods (Paper V), we see how the understanding regarding ML itself is incomplete (Paper VI). It is the hope of the author that those observations would lead to a deeper understanding of the data-driven models, and after all, of the physical world and ourselves.

6. Ackowledgements

Enlightenment is man's emergence from his self-incurred immaturity. Immaturity is the inability to use one's own understanding without the guidance of another.[153]

Immanuel Kant

This thesis is my humble attempt to carve down my understanding, and this is obviously impossible without the help of others, to whom I owe my gratitude. I shall begin with those who have led me in the journey, who have shown me the tracks and footprints to follow, who have taught me the norms and kept me from the traps. Thanks to my supervisors Chao, Peter, and Carl, you have been excellent and patient teachers and the most solid support in my first-ever long travel.

I would also like to thank all the members of the TEOROO/CMC group, whose company made the trip feels shorter. Thank you, Kersti, for leading this fantastic group for scientific discourse and for your always generous opinions. Thanks to Pavlin and Jolla, discussions with you never cease to interest me. A special thanks to Harish, Lisanne, Linnéa, and Thomas, who have helped to proofread the thesis and have been a pleasure to collaborate with. I shall extend my thanks to other members of the structural chemistry programme for the vibrant scientific development that has been instructive to me. Thanks, Simon, for being the most welcoming friend to a simulant, and for all the fruitful discussions.

I save my most sincere thanks to my parents, grandparents, and family for fostering this peculiar mind, enduring his stubbornness, and protecting his curiosity this far. And my deepest gratitude goes to the one who has put up with the most of my indulgence.

7. Sammanfattning på svenska: Att förstå jontransporter i elektrolyter

Jonledare är väsentliga komponenter i många biologiska och teknologiska sammanhang. Ett aktuellt och viktigt exempel rör dagens elektrifierade samhälle. När en portabel elektrisk enhet, såsom din smartphone eller laptop, förbrukar el, så förbrukas "negativa laddningar" (elektroner) i batteriet. I batteriet kompenseras denna laddningsförlust genom att samma mängd joner rör sig i motsatt riktning mellan anoden och katoden inuti batteriet. Jonerna rör sig då genom ett jonledande material som separerar de olika elektroderna.

Vad är då en jon? Joner är små partiklar, vilka kan vara antingen laddade atomer, eller laddade mindre molekyler. Joner är storleksmässigt cirka en miljard gånger mindre än batteriet i din telefon. Det var den svenske vetenskapsmannen Svante Arrhenius som först insåg att salter (de så kallade elektrolyterna) bildar joner när de löses i vatten.

När joner rör sig genom ett jonledande material, t.ex. i ett batteri, så förbrukar det också en del energi vilket minskar dess effektivitet. För att kunna tillverka bättre material till dagens och framtidens batterier är det därför viktigt att förstå hur joner påverkas av elektriska fält, och då särskilt hur olika joner interagerar med varandra när de rör sig tillsammans. Albert Einstein visade tidigt i sin karriär att vi kan ta reda på hur joner rör sig under elektriska fält genom att titta på hur de slumpmässigt rör sig utan det elektriska fältet. Teorin utvidgades sedan till att även beskriva den ömsesidiga interaktionen mellan joner och deras korrelerade rörelse.

Tyvärr är joner för små för att kunna spåras eller ens synas med blotta ögat, eller ens med avancerade experimentella metoder, men tack vare kvantmekaniken vet vi ändå hur de rör sig. Hur de rör sig kan simuleras genom så kallad molekyldynamik i datorer. I sådana simuleringar studeras en liten bit av materialet som ändå är representativt för materialets egenskaper. Denna teknik för simulering och tillhörande teorier har utvecklats för att säkerställa att den mikroskopiska simuleringen matchar det som verkligen händer i ett verkligt fall. För att få tillförlitliga resultat krävs att en simulering besöker alla möjliga tillstånd och att jonerna som vi är intresserade av interagerar med sin omgivning på ett realistiskt sätt, vilket medför att vi måste simulera systemen under lång tid. Problemet med dagens tekniker är att de kvantmekaniska ekvationerna är komplexa och därmed svåra och ofta tidsödande att lösa även för en dator. Det gör att vi i normalfallet inte kan observera partiklarna tillräckligt länge för att ge en korrekt beskrivning.

Ett sätt att påskynda beräkningarna är att förenkla de kvantmekaniska modellerna, t.ex. genom att beskriva interaktioner mellan joner och atomer med osynliga "fjädrar". Dessa modeller kallas för kraftfältsmodeller (engelska: Force Field models). Den första delen i denna avhandling använder just sådana modeller för att studera jontransport i flera olika elektrolyter. Med datorsimuleringar kan vi tydligt studera rörelsen av joner och hur de interagerar med varandra. I artikel I visade jag hur jonernas korrelation i första hand bestäms av materialets viskositet. Detta resultat verifierades genom att studera en serie experiment utförda för en klass av elektrolyter som kallas joniska vätskor.

Datorsimuleringar ger möjligheten att föreställa oss vad som händer om vi justerar egenskaperna av de ingående kemikalierna bortom de experimentella förutsättningarna. I min avhandling använder jag denna teknik för att studera polymerelektrolyter. I artikel II visade jag att genom att justera polariteten hos polymerelektrolyten, så påverkades livstiden för parbildning av joner med motsatta laddningar. En viktig upptäckt var att de jonpar som har en längre livstid rör sig tillsammans, och de som lever kortare tenderar att gå i motsatta riktningar.

Även om detta resultat inte är intuitivt, är det faktiskt rimligt. Detta beror på att vi måste definiera en referensram innan vi pratar om rörelse. I en simulering definieras referensramen med ett masscentrum så att tunga joner tenderar att röra sig mot varandra. I experiment är det dock bekvämare att mäta rörelsen med lösningsmedlet som referens. I artikel III överkom vi denna begreppsklyfta genom att visa att simulering överensstämmer med experiment endast om vi konverterar resultaten på ett korrekt sätt till samma referensram.

I de tidigare fallen har jag tittat på joner som inte reagerar med sin omgivning, t.ex. lösningsmedlet. Ett exempel är när vi simulerar en vattenlösning innehållande lut (NaOH). Vi vet att jonerna som bildas i vattenlösningen kan röra sig mycket snabbt p.g.a. att de kan reagera med vattenmolekyler. För att simulera deras rörelser behövs sofistikerade kraftfältsmodeller som även kan hantera kemiska reaktioner på ett korrekt sätt, d.v.s. bildandet och brytande av interna kemiska bindningar. I den andra halvan av denna avhandling tar jag hjälp av maskininlärning för att utföra sådana simuleringar. Istället för att göra förenklade modeller baserade på fysikens lagar, designar jag algoritmer som läser kvantmekaniska beräkningar, och därigenom förutsäger atomernas rörelser. Metoden är egentligen inte ny, utan är nästan lika gammal som digitala datorer, men det är först nyligen som den har blivit tillräckligt kraftfull för att lösa realistiska problem. I artikel IV testade jag detta tillvägagångssätt för lutlösningar av olika koncentrationer. Jag visade att kraftfältsmodellen förutsäger korrekt hur den kemiska reaktionen mellan lut och vatten påskyndar jontransporten vid olika temperaturer.

Maskininlärningsmetoden som användes i artikel IV visade sig vara väldigt användbar, men den kräver fortfarande mycket insikt om vad som är viktigt i det simulerade kemiska systemet. I artikel V förbättrade jag maskininlärningsalgoritmen genom att låta den lära sig kemiska interaktioner på ett mer

allmänt sätt. Modellen instrueras att göra förutsägelser genom att bygga upp en serie begrepp där vart och ett beror på tidigare begrepp genom ett strukturellt så kallat artificiellt neuronnät. Dessa modeller kan tränas att matcha data från kvantmekaniska beräkningar. Det som skiljer mot tidigare kraftfältsformuleringar är att vi nu kan mer generellt förutsäga egenskaper och rörelsemönster hos olika material utan någon specifik modelldesign.

Trots de enorma fördelar som maskininlärningsmodeller har när det gäller flexibilitet, så påvisade jag i en följande studie en svaghet. Maskininlärningsmodeller opererar i ett högdimensionellt rum, med en så hög dimension att vi inte kan vara riktigt säkra på att vi fyller rummet med tillräckligt med data. En bra liknelse är när vi bakar bröd. När "degen" (data) inte kan fylla hela "brödet" (rummet) får vi problem. Dessa hålrum är svåra att upptäcka under modellens uppbyggnad, och kan leda till mycket dåliga modeller. I artikel VI, utvecklade jag modeller för att simulera vatten. Ett problem var att vissa modeller gav en alltför låg kokpunkt för det simulerade vattnet, som kokade redan vid rumstemperatur. Mina studier pekade i riktningen på att traningsalgoritmen var orsaken till problemet, d.v.s. hur vi "bakade" brödet från degen, snarare än "degen" själv. Det är dock fortfarande oklart hur "träningen" faktiskt går till, och därför också, vilken som är den bästa träningsalgoritmen.

I det sista arbetet (artikel VII) försöker jag lösa träningsproblemet med maskininlärningsmodeller genom att använda en adaptiv "lärande-i-farten" algoritm för att automatiskt upptäcka när en modell kommer in i ett ihåligt område och då lägger till data när detta händer. Slutligen tillåter detta oss att köra mycket långa simuleringar, vilket behövs för att bestämma diffusionskoefficienter i det protonledande joniska flytande materialet, där protonen kan hoppa från en molekyl till en annan. Intressant nog, när vi tittar på klusterstrukturen i vår maskininlärningsmodell, så kan vi följa hur denna förändras när vi lägger till mer och mer data mot en som liknar den som vi har från vår kemiska intuition.

Sammantaget tar denna avhandling en djupdykning i den mikroskopiska världen av elektrolyter och ger användbar information om hur dessa presterar i elektrokemiska tillämpningar. För att studera elektrolyterna har nya metoder som drar fördel av maskininlärning utvecklats, och deras prestanda har blivit noggrant testade. Slutsatsen från dessa studier är att med en noggrann design och träningsprocedur fås kemiskt intuitiva modeller som tillåter oss att simulera komplexa reaktiva system av atomer och bestämma deras jontransportegenskaper.

Bibliography

[1] J. O. Bockris, B. E. Conway, E. Yeager, and R. E. White, eds., *Comprehensive treatise of electrochemistry, Electrochemical energy conversion and storage*, Vol. 3 (Plenum Press, 1981).

[2] P. Simon and Y. Gogotsi, "Capacitive energy storage in nanostructured carbon–electrolyte systems", Accounts Chem. Res. **46**, 1094–1103 (2012).

[3] C. Sångeland, J. Mindemark, R. Younesi, and D. Brandell, "Probing the interfacial chemistry of solid-state lithium batteries", Solid State Ion. **343**, 115068 (2019).

[4] X.-H. Yang, M. Papasizza, A. Cuesta, and J. Cheng, "Water-in-salt environment reduces the overpotential for reduction of CO_2 to CO_2^- in ionic liquid/water mixtures", ACS Catalysis, 6770–6780 (2022).

[5] K. Xu, "Electrolytes and interphases in Li-ion batteries and beyond", Chem. Rev. **114**, 11503–11618 (2014).

[6] A. A. Franco et al., "Boosting rechargeable batteries R&D by multiscale modeling: myth or reality?", Chem. Rev **119**, 4569–4627 (2019).

[7] S. Fleischmann et al., "Pseudocapacitance: from fundamental understanding to high power energy storage materials", Chem. Rev. **120**, 6738–6782 (2020).

[8] A. Z. Weber and J. Newman, "Modeling transport in polymer-electrolyte fuel cells", Chem. Rev. **104**, 4679–4726 (2004).

[9] E. Flores et al., "Learning the laws of lithium-ion transport in electrolytes using symbolic regression", Digit. Discov. **1**, 440–447 (2022).

[10] M. Korth, "Large-scale virtual high-throughput screening for the identification of new battery electrolyte solvents: evaluation of electronic structure theory methods", Phys. Chem. Chem. Phys. **16**, 7919–7926 (2014).

[11] Y. Shao, L. Knijff, F. M. Dietrich, K. Hermansson, and C. Zhang, "Modelling bulk electrolytes and electrolyte interfaces with atomistic machine learning", Batter. Supercaps. **4**, 585–595 (2021).

[12] W. Xu, E. I. Cooper, and C. A. Angell, "Ionic liquids: ion mobilities, glass temperatures, and fragilities", J. Phys. Chem. B **107**, 6170–6178 (2003).

[13] K. Xu, "Nonaqueous liquid electrolytes for lithium-based rechargeable batteries", Chem. Rev. **104**, 4303–4418 (2004).

[14] J. Mindemark, M. J. Lacey, T. Bowden, and D. Brandell, "Beyond PEO—alternative host materials for Li^+-conducting solid polymer electrolytes", Prog. Polym. Sci. **81**, 114–143 (2018).

[15] R. A. Robinson and R. H. Stokes, *Electrolyte solutions*, 2nd ed. (Butterworths, 1965).

[16] P. G. Bruce and C. A. Vincent, "Steady state current flow in solid binary electrolyte cells", J. Electroanal. Chem. Interfacial Electrochem. **225**, 1–17 (1987).

[17] M. Holz, "Electrophoretic NMR", Chem. Soc. Rev. **23**, 165–174 (1994).

[18] L. Onsager, *The motion of ions: principles and concepts*, Nobel Lecture, Dec. 1968.

[19] P. Debye and E. Hückel, "Zur theorie der elektrolyte. I. gefrierpunktserniedrigung und verwandte erscheinungen", Phys. Z **24**, 185–206 (1923).

[20] L. Onsager and R. M. Fuoss, "Irreversible processes in electrolytes. diffusion, conductance and viscous flow in arbitrary mixtures of strong electrolytes", J. Phys. Chem. **36**, 2689–2778 (1932).

[21] W. Ebeling and J. Rose, "Conductance theory of concentrated electrolytes in an MSA-type approximation", J. Solution Chem. **10**, 599–609 (1981).

[22] O. Bernard, W. Kunz, P. Turq, and L. Blum, "Conductance in electrolyte solutions using the mean spherical approximation", J. Phys. Chem. **96**, 3833–3840 (1992).

[23] A. R. Altenberger and H. L. Friedman, "Theory of conductance and related isothermal transport coefficients in electrolytes", J. Chem. Phys. **78**, 4162–4173 (1983).

[24] A. Chandra and B. Bagchi, "Frequency dependence of ionic conductivity of electrolyte solutions", J. Chem. Phys. **112**, 1876–1886 (2000).

[25] J. Wu and Z. Li, "Density-functional theory for complex fluids", Annu. Rev. Phys. Chem. **58**, 85–112 (2007).

[26] A. Anderko, P. Wang, and M. Rafal, "Electrolyte solutions: from thermodynamic and transport property models to the simulation of industrial processes", Fluid Phase Equilibr. **194-197**, 123–142 (2002).

[27] T. Xiao and X. Song, "A systematic way to extend the Debye–Hückel theory beyond dilute electrolyte solutions", J. Phys. Chem. A **125**, 2173–2183 (2021).

[28] P. Yatsyshin, S. Kalliadasis, and A. B. Duncan, "Physics-constrained bayesian inference of state functions in classical density-functional theory", J. Chem. Phys. **156**, 074105 (2022).

[29] D. R. MacFarlane et al., "On the concept of ionicity in ionic liquids", Phys. Chem. Chem. Phys. **11**, 4962–4967 (2009).

[30] J. Maier, "Mass transport in the presence of internal defect reactions-concept of conservative ensembles: I, chemical diffusion in pure compounds", J. Am. Ceram. Soc. **76**, 1212–1217 (1993).

[31] F. M. Gray and P. G. Bruce, "Polymer electrolytes II: physical principles", in *Solid state electrochemistry*, edited by P. G. Bruce (Cambridge University Press, 1994), pp. 119–162.

[32] G. W. Driver et al., "Correlated/non-correlated ion dynamics of charge-neutral ion couples: the origin of ionicity in ionic liquids", Phys. Chem. Chem. Phys. **19**, 4975–4988 (2017).

[33] J. Landesfeind and H. A. Gasteiger, "Temperature and concentration dependence of the ionic transport properties of lithium-ion battery electrolytes", J. Electrochem. Soc. **166**, A3079–A3097 (2019).

[34] B. Kirchner, F. Malberg, D. S. Firaha, and O. Hollóczki, "Ion pairing in ionic liquids", J. Phys.: Condens. Matter **27**, 463002 (2015).

[35] N. Molinari, J. P. Mailoa, and B. Kozinsky, "Effect of salt concentration on ion clustering and transport in polymer solid electrolytes: a molecular dynamics study of PEO–LiTFSI", Chem. Mater. **30**, 6298–6306 (2018).

[36] A. France-Lanord and J. C. Grossman, "Correlations from ion pairing and the Nernst-Einstein equation", Phys. Rev. Lett. **122**, 136001 (2019).

[37] N. H. C. Lewis et al., "Signatures of ion pairing and aggregation in the vibrational spectroscopy of super-concentrated aqueous lithium bistriflimide solutions", J. Phys. Chem. C **124**, 3470–3481 (2020).

[38] M.-M. Walz and D. van der Spoel, "Microscopic origins of conductivity in molten salts unraveled by computer simulations", Commun. Chem. **4**, 9 (2021).

[39] H. K. Kashyap, H. V. R. Annapureddy, F. O. Raineri, and C. J. Margulis, "How is charge transport different in ionic liquids and electrolyte solutions?", J. Phys. Chem. B **115**, 13212–13221 (2011).

[40] J. G. McDaniel and C. Y. Son, "Ion correlation and collective dynamics in BMIM/BF$_4$-based organic electrolytes: from dilute solutions to the ionic liquid limit", J. Phys. Chem. B **122**, 7154–7169 (2018).

[41] N. M. Vargas-Barbosa and B. Roling, "Dynamic ion correlations in solid and liquid electrolytes: how do they affect charge and mass transport?", ChemElectroChem **7**, 367–385 (2019).

[42] W. S. Loo, C. Fang, N. P. Balsara, and R. Wang, "Uncovering local correlations in polymer electrolytes by X-ray scattering and molecular dynamics simulations", Macromolecules **54**, 6639–6648 (2021).

[43] M.-M. Walz and D. van der Spoel, "Direct link between structure, dynamics, and thermodynamics in molten salts", J. Phys. Chem. C **123**, 25596–25602 (2019).

[44] J. J. Molina, J.-F. Dufrêche, M. Salanne, O. Bernard, and P. Turq, "Primitive models of ions in solution from molecular descriptions: a perturbation approach", J. Chem. Phys. **135**, 234509 (2011).

[45] M. Tuckerman, K. Laasonen, M. Sprik, and M. Parrinello, "Ab initio molecular dynamics simulation of the solvation and transport of hydronium and hydroxyl ions in water", J. Chem. Phys. **103**, 150–161 (1995).

[46] M. E. Tuckerman, D. Marx, and M. Parrinello, "The nature and transport mechanism of hydrated hydroxide ions in aqueous solution", Nature **417**, 925–929 (2002).

[47] J. Ingenmey, S. Gehrke, and B. Kirchner, "How to harvest grotthuss diffusion in protic ionic liquid electrolyte systems", ChemSusChem **11**, 1900–1910 (2018).

[48] H. Watanabe et al., "Possible proton conduction mechanism in pseudo-protic ionic liquids: a concept of specific proton conduction", J. Phys. Chem. B **123**, 6244–6252 (2019).

[49] O. Hollóczki, F. Malberg, T. Welton, and B. Kirchner, "On the origin of ionicity in ionic liquids. ion pairing versus charge transfer", Phys. Chem. Chem. Phys. **16**, 16880–16890 (2014).

[50] J. Behler and M. Parrinello, "Generalized neural-network representation of high-dimensional potential-energy surfaces", Phys. Rev. Lett. **98**, 146401 (2007).

[51] A. P. Bartók, M. C. Payne, R. Kondor, and G. Csányi, "Gaussian approximation potentials: the accuracy of quantum mechanics, without the electrons", Phys. Rev. Lett. **104**, 136403 (2010).

[52] M. A. Caro, "Optimizing many-body atomic descriptors for enhanced computational performance of machine learning based interatomic potentials", Phys. Rev. B **100**, 024112 (2019).

[53] Y. Zuo et al., "Performance and cost assessment of machine learning interatomic potentials", J. Phys. Chem. A **124**, 731–745 (2020).

[54] J. Goodenough, "Ceramic solid electrolytes", Solid State Ion. **94**, 17–25 (1997).

[55] M. Doyle and J. Newman, "Analysis of transference number measurements based on the potentiostatic polarization of solid polymer electrolytes", J. Electrochem. Soc. **142**, 3465 (1995).

[56] R. E. Oesper and M. Speter, "The Faraday-Whewell correspondence concerning electro-chemical terms", Sci. Mon. **45**, 535–546 (1937).

[57] B. Cantor, "Svante Arrhenius", in *Equations of materials* (Oxford University Press, 2020), pp. 94–100.

[58] A. Einstein, *Investigations on the theory of the Brownian movement* (Dover Publications, 1956).

[59] D. G. Miller, "Application of irreversible thermodynamics to electrolyte solutions. I. determination of ionic transport coefficients l_{ij} for isothermal vector transport processes in binary electrolyte systems", J. Phys. Chem. **70**, 2639–2659 (1966).

[60] J. Newman and N. P. Balsara, *Electrochemical systems* (Wiley, 2020).

[61] L. Onsager, "Reciprocal relations in irreversible processes. I.", Phys. Rev. **37**, 405–426 (1931).

[62] H. J. V. Tyrrell and K. R. Harris, *Diffusion in liquids, A theoretical and experimental study* (Butterworths, 1984).

[63] C. F. Curtiss and R. B. Bird, "Multicomponent diffusion", Ind. Eng. Chem. Res. **38**, 2515–2522 (1999).

[64] D. R. Wheeler and J. Newman, "Molecular dynamics simulations of multicomponent diffusion. 1. equilibrium method", J. Phys. Chem. B **108**, 18353–18361 (2004).

[65] M. Tuckerman, *Statistical mechanics, Theory and molecular simulation* (Oxford University Press, Apr. 2010).

[66] S. R. de Groot and P. Mazur, *Non-equilibrium thermodynamics* (Dover Publications, 1984).

[67] D. G. Miller, "Thermodynamics of irreversible processes. the experimental verification of the Onsager reciprocal relations.", Chem. Rev. **60**, 15–37 (1960).

[68] J. O. Bockris, B. E. Conway, and E. Yeager, eds., *Comprehensive treatise of electrochemistry, Thermodynamic and transport properties of aqueous and molten electrolytes*, Vol. 5 (Plenum Press, 1983).

[69] G. K. Batchelor, "Kinematics of the flow field", in *An introduction to fluid dynamics* (Cambridge University Press, 2000), pp. 71–130.

[70] J.-F. Dufrêche, O. Bernard, and P. Turq, "Transport equations for concentrated electrolyte solutions: reference frame, mutual diffusion", J. Chem. Phys. **116**, 2085–2097 (2002).

[71] N. Bjerrum, *Niels Bjerrum selected papers* (Einar Munksgaard, 1949).

[72] M. Ceriotti et al., "Nuclear quantum effects in water and aqueous systems: experiment, theory, and current challenges", Chem. Rev. **116**, 7529–7550 (2016).

[73] A. Rahman, "Correlations in the motion of atoms in liquid argon", Phys. Rev. **136**, A405–A411 (1964).

[74] A. Rahman and F. H. Stillinger, "Propagation of sound in water. a molecular-dynamics study", Phys. Rev. A **10**, 368–378 (1974).

[75] H. C. Andersen, "Molecular dynamics simulations at constant pressure and/or temperature", J. Chem. Phys. **72**, 2384–2393 (1980).

[76] F. Pulizzi, "A method to break all barriers", Nat. Mater. **9**, 693–694 (2010).

[77] B. Leimkuhler and C. Matthews, *Molecular dynamics with deterministic and stochastic numerical methods* (Springer, 2015).

[78] D. J. Evans and G. P. Morriss, *Statistical mechanics of nonequilibrium liquids* (ANU E Press, 2007).

[79] G. J. Martyna, M. L. Klein, and M. Tuckerman, "Nosé–Hoover chains: the canonical ensemble via continuous dynamics", J. Chem. Phys. **97**, 2635–2643 (1992).

[80] M. Parrinello and A. Rahman, "Polymorphic transitions in single crystals: a new molecular dynamics method", J. Appl. Phys. **52**, 7182–7190 (1981).

[81] S. E. Feller, Y. Zhang, R. W. Pastor, and B. R. Brooks, "Constant pressure molecular dynamics simulation: the Langevin piston method", J. Chem. Phys. **103**, 4613–4621 (1995).

[82] G. Bussi, D. Donadio, and M. Parrinello, "Canonical sampling through velocity rescaling", J. Chem. Phys. **126**, 014101 (2007).

[83] J. G. Kirkwood and J. Riseman, "The intrinsic viscosities and diffusion constants of flexible macromolecules in solution", J. Chem. Phys. **16**, 565–573 (1948).

[84] B. Dünweg and K. Kremer, "Molecular dynamics simulation of a polymer chain in solution", J. Chem. Phys. **99**, 6983–6997 (1993).

[85] I.-C. Yeh and G. Hummer, "System-size dependence of diffusion coefficients and viscosities from molecular dynamics simulations with periodic boundary conditions", J. Phys. Chem. B **108**, 15873–15879 (2004).

[86] B. S. Daan Frenkel, *Understanding molecular simulation* (Elsevier, 2001).

[87] R. W. Hockney and J. W. Eastwood, *Computer simulation using particles* (CRC Press, 1988).

[88] M. J. Hwang, T. P. Stockfisch, and A. T. Hagler, "Derivation of class II force fields. 2. derivation and characterization of a class II force field, CFF93, for the alkyl functional group and alkane molecules", J. Am. Chem. Soc. **116**, 2515–2525 (1994).

[89] F. Ercolessi and J. B. Adams, "Interatomic potentials from first-principles calculations: the force-matching method", EPL **26**, 583–588 (1994).

[90] T. P. Senftle et al., "The ReaxFF reactive force-field: development, applications and future directions", npj Comput. Mater. **2**, 15011 (2016).

[91] J. E. Lennard-Jones, "Cohesion", Proc. Phys. Soc. **43**, 461–482 (1931).

[92] S. C. Wang, "Die gegenseitige einwirkung zweier wasserstoffatome", Phys. Z. **28**, 663–666 (1927).

[93] R. Eisenschitz and F. London, "Über das verhältnis der van der Waalsschen kräfte zu den homöopolaren bindungskräften.", Z. Phys. **60**, 491–527 (1930).

[94] J. S. Rowlinson, *Cohesion, A scientific history of intermolecular forces* (Cambridge University Press, 2002).

[95] A. Szabo and N. S. Ostlund, *Modern quantum chemistry, Introduction to advanced electronic structure theory* (Dover Publications, 1996).

[96] T. Helgaker, P. Jorgensen, and J. Olsen, *Molecular electronic-structure theory* (Wiley, 2000).

[97] P. Hohenberg and W. Kohn, "Inhomogeneous electron gas", Phys. Rev. **136**, B864–B871 (1964).

[98] W. Kohn and L. J. Sham, "Self-consistent equations including exchange and correlation effects", Phys. Rev. **140**, A1133–A1138 (1965).

[99] J. P. Perdew, "Jacob's ladder of density functional approximations for the exchange-correlation energy", in AIP conference proceedings (2001).

[100] Y. Zhao and D. G. Truhlar, "The M06 suite of density functionals for main group thermochemistry, thermochemical kinetics, noncovalent interactions, excited states, and transition elements: two new functionals and systematic testing of four M06-class functionals and 12 other functionals", Theor. Chem. Acc. **120**, 215–241 (2007).

[101] K. Yang, J. Zheng, Y. Zhao, and D. G. Truhlar, "Tests of the RPBE, revPBE, τ-HCTHhyb, ωb97x-d, and MOHLYP density functional approximations and 29 others against representative databases for diverse bond energies and barrier heights in catalysis", J. Chem. Phys. **132**, 164117 (2010).

[102] A. J. Cohen, P. Mori-Sánchez, and W. Yang, "Challenges for density functional theory", Chem. Rev. **112**, 289–320 (2011).

[103] G. Kebede, P. D. Mitev, P. Broqvist, A. Eriksson, and K. Hermansson, "Fifty shades of water: benchmarking DFT functionals against experimental data for ionic crystalline hydrates", J. Chem. Theory. Comput. **15**, 584–594 (2018).

[104] R. Car and M. Parrinello, "Unified approach for molecular dynamics and density-functional theory", Phys. Rev. Lett. **55**, 2471–2474 (1985).

[105] T. D. Kühne et al., "CP2k: an electronic structure and molecular dynamics software package - quickstep: efficient and accurate electronic structure calculations", J. Chem. Phys. **152**, 194103 (2020).

[106] A. M. N. Niklasson, "Extended lagrangian Born–Oppenheimer molecular dynamics for orbital-free density-functional theory and polarizable charge equilibration models", J. Chem. Phys. **154**, 054101 (2021).

[107] Y.-L. S. Tse, C. Knight, and G. A. Voth, "An analysis of hydrated proton diffusion in ab initio molecular dynamics", J. Chem. Phys. **142**, 014104 (2015).

[108] V. F. Rozsa and G. Galli, "Molecular polarizabilities in aqueous systems from first-principles", J. Phys. Chem. B **125**, 2183–2192 (2021).

[109] M. L. Minsky and S. A. Papert, *Perceptrons - expanded edition, An introduction to computational geometry* (MIT Press, 1987).

[110] K. Hornik, M. Stinchcombe, and H. White, "Multilayer feedforward networks are universal approximators", Neural Netw. **2**, 359–366 (1989).

[111] Y. Lecun and Y. Bengio, "Convolutional networks for images, speech, and time-series", in *The handbook of brain theory and neural networks*, edited by M. Arbib (MIT Press, 1995).

[112] A. Krizhevsky, I. Sutskever, and G. E. Hinton, "Imagenet classification with deep convolutional neural networks", in Advances in neural information processing systems, Vol. 25, edited by F. Pereira, C. Burges, L. Bottou, and K. Weinberger (2012).

[113] S. Hochreiter and J. Schmidhuber, "Long short-term memory", Neural Comput. **9**, 1735–1780 (1997).

[114] F. A. Faber, A. S. Christensen, B. Huang, and O. A. von Lilienfeld, "Alchemical and structural distribution based representation for universal quantum machine learning", J. Chem. Phys. **148**, 241717 (2018).

[115] M. J. Willatt, F. Musil, and M. Ceriotti, "Atom-density representations for machine learning", J. Chem. Phys. **150**, 154110 (2019).

[116] R. Drautz, "Atomic cluster expansion for accurate and transferable interatomic potentials", Phys. Rev. B **99**, 014104 (2019).

[117] S. N. Pozdnyakov, L. Zhang, C. Ortner, G. Csányi, and M. Ceriotti, "Local invertibility and sensitivity of atomic structure-feature mappings", (2021), `arXiv: 2109.11440`.

[118] D. P. Kovács et al., "Linear atomic cluster expansion force fields for organic molecules: beyond RMSE", J. Chem. Theory Comput. **17**, 7696–7711 (2021).

[119] J. Vandermause et al., "On-the-fly active learning of interpretable bayesian force fields for atomistic rare events", npj Comput. Mater. **6**, 20 (2020).

[120] R. Jinnouchi, F. Karsai, and G. Kresse, "On-the-fly machine learning force field generation: application to melting points", Phys. Rev. B **100**, 014105 (2019).

[121] Y. Zhang et al., "DP-GEN: a concurrent learning platform for the generation of reliable deep learning based potential energy models", Comput. Phys. Commun. **253**, 107206 (2020).

[122] C. van der Oord, M. Sachs, D. P. Kovács, C. Ortner, and G. Csányi, "Hyperactive learning (HAL) for data-driven interatomic potentials", (2022), arXiv: 2210.04225.

[123] N. A. Stolwijk, J. Kösters, M. Wiencierz, and M. Schönhoff, "On the extraction of ion association data and transference numbers from ionic diffusivity and conductivity data in polymer electrolytes", Electrochim. Acta. **102**, 451–458 (2013).

[124] H. Tokuda, S. Tsuzuki, M. A. B. H. Susan, K. Hayamizu, and M. Watanabe, "How ionic are room-temperature ionic liquids? an indicator of the physicochemical properties", J. Phys. Chem. B **110**, 19593–19600 (2006).

[125] H. Tokuda, K. Hayamizu, K. Ishii, M. A. B. H. Susan, and M. Watanabe, "Physicochemical properties and structures of room temperature ionic liquids. 2. variation of alkyl chain length in imidazolium cation", J. Phys. Chem. B **109**, 6103–6110 (2005).

[126] H. Tokuda et al., "Physicochemical properties and structures of room-temperature ionic liquids. 3. variation of cationic structures", J. Phys. Chem. B **110**, 2833–2839 (2006).

[127] H. Gudla, C. Zhang, and D. Brandell, "Effects of solvent polarity on Li-ion diffusion in polymer electrolytes: an all-atom molecular dynamics study with charge scaling", J. Phys. Chem. B **124**, 8124–8131 (2020).

[128] D. Laage and J. T. Hynes, "On the residence time for water in a solute hydration shell: application to aqueous halide solutions", J. Phys. Chem. B **112**, 7697–7701 (2008).

[129] V. Gold, ed., *The IUPAC compendium of chemical terminology* (IUPAC, 2019).

[130] D. M. Pesko et al., "Negative transference numbers in poly(ethylene oxide)-based electrolytes", J. Electrochem. Soc. **164**, E3569–E3575 (2017).

[131] M. P. Rosenwinkel and M. Schönhoff, "Lithium transference numbers in PEO/LiTFSA electrolytes determined by electrophoretic NMR", J. Electrochem. Soc. **166**, A1977–A1983 (2019).

[132] I. Villaluenga et al., "Negative Stefan-Maxwell diffusion coefficients and complete electrochemical transport characterization of homopolymer and block copolymer electrolytes", J. Electrochem. Soc. **165**, A2766–A2773 (2018).

[133] D. G. Miller, "Some comments on multicomponent diffusion: negative main term diffusion coefficients, second law constraints, solvent choices, and reference frame transformations", J. Phys. Chem. **90**, 1509–1519 (1986).

[134] D. Marx, "Proton transfer 200 years after von Grotthuss: insights from ab initio simulations", ChemPhysChem **7**, 1848–1870 (2006).

[135] T. J. F. Day, U. W. Schmitt, and G. A. Voth, "The mechanism of hydrated proton transport in water", J. Am. Chem. Soc. **122**, 12027–12028 (2000).

[136] A. Warshel and R. M. Weiss, "An empirical valence bond approach for comparing reactions in solutions and in enzymes", J. Am. Chem. Soc. **102**, 6218–6226 (1980).

[137] W. Zhang and A. C. T. van Duin, "ReaxFF reactive molecular dynamics simulation of functionalized poly(phenylene oxide) anion exchange membrane", J. Phys. Chem. C **119**, 27727–27736 (2015).

[138] M. Hellström and J. Behler, "Concentration-dependent proton transfer mechanisms in aqueous NaOH solutions: from acceptor-driven to donor-driven and back", J. Phys. Chem. Lett. **7**, 3302–3306 (2016).

[139] H. W. Kuhn, "The Hungarian method for the assignment problem", Nav. Res. Logist. Q. **2**, 83–97 (1955).

[140] K. T. Schütt, H. E. Sauceda, P.-J. Kindermans, A. Tkatchenko, and K.-R. Müller, "SchNet – a deep learning architecture for molecules and materials", J. Chem. Phys. **148**, 241722 (2018).

[141] Y. Shao, L. Andersson, L. Knijff, and C. Zhang, "Finite-field coupling via learning the charge response kernel", Electron. Struct. **4**, 014012 (2022).

[142] R. Ramakrishnan, P. O. Dral, M. Rupp, and O. A. von Lilienfeld, "Quantum chemistry structures and properties of 134 kilo molecules", Sci. Data, 140022 (2014).

[143] I. E. Castelli et al., "Computational screening of perovskite metal oxides for optimal solar light capture", Energy Environ. Sci. **5**, 5814–5819 (2012).

[144] T. Morawietz, A. Singraber, C. Dellago, and J. Behler, "How van der Waals interactions determine the unique properties of water", Proc. Natl. Acad. Sci. U.S.A **113**, 8368–8373 (2016).

[145] J. Behler, "RuNNer – a neural network code for high-dimensional potential-energy surfaces", Universität Göttingen (2018).

[146] D. P. Kingma and J. Ba, "Adam: a method for stochastic optimization", (2014), `arXiv: 1412.6980`.

[147] J. Martens and R. Grosse, "Optimizing neural networks with Kronecker-factored approximate curvature", (2015), `arXiv: 1503.05671`.

[148] A. G. Wills and T. B. Schön, "Stochastic quasi-Newton with line-search regularisation", Automatica **127**, 109503 (2021).

[149] B. Cheng, E. A. Engel, J. Behler, C. Dellago, and M. Ceriotti, "Ab initio thermodynamics of liquid and solid water", Proc. Natl. Acad. Sci. U.S.A **116**, 1110–1115 (2019).

[150] C. Zhang, S. Bengio, M. Hardt, B. Recht, and O. Vinyals, "Understanding deep learning requires rethinking generalization", (2016), `arXiv: 1611.03530`.

[151] Y. Jiang, B. Neyshabur, H. Mobahi, D. Krishnan, and S. Bengio, "Fantastic generalization measures and where to find them", (2019), `arXiv: 1912.02178`.

[152] T. Morawietz, "Efficient simulations of water with *ab initio* accuracy", Doctoral Thesis (Ruhr-Universität Bochum, Universitätsbibliothek, 2016).

[153] I. Kant, *Answer to the question 'what is enlightenment?'* (Penguin Books, 2009).

Acta Universitatis Upsaliensis

Digital Comprehensive Summaries of Uppsala Dissertations
from the Faculty of Science and Technology 2210

Editor: The Dean of the Faculty of Science and Technology